Internship report Grenoble-INP Ense3/Phelma

SICOM section   2022/2023

Pierre GASPARI

Searching FRBs with NenuFAR

March to August 2023

École Nationale Supérieure
de l'Énergie, l'Eau et l'Environnement
ENSE3

Bât, Grenoble INP - GreEn-ER
21 Av. des Martyrs
38031 Grenoble, France
+33 4 76 82 62 00
https://ense3.grenoble-inp.fr/

École Nationale Supérieure
de Physique, Electronique, Materiaux
PHELMA

3 Parv. Louis Néel,
38000 Grenoble, France
+33 4 56 52 91 00
https://phelma.grenoble-inp.fr/

Under the supervision of:

CNRS Tutor:
Ph.D, Cherry Ng
cherrywyng@gmail.com

CNRS Tutor:
Ph.D, Jean-Mathias Griessmeier
jean-mathias.griessmeier@cnrs-orleans.fr

Referent teacher:
Ph.D, Ronald Phlypo
ronald.phlypo@grenoble-inp.fr

Summary

English Summary

The aim of the project was to search for Fast Radio Bursts (FRBs) using data from the Nenu-FAR radio telescope within the ASTRO team at the CNRS Orléans. The study of FRBs, extragalactic emissions, opens up important prospects for a better understanding of the universe that surrounds us. With the recent appearance of new radio telescopes capable of detecting them, this phenomenon is expanding. Against this background, this project was launched with the aim of identifying FRBs in frequency ranges where they have never been detected before (low frequencies, from 30 MHz to 80 MHz). A model of FRBs was created to represent their physical properties and the physical phenomena that characterise them at these frequencies. The development of a pipeline was crucial to manage the interference present in the radio telescope observations. This pipeline was designed to optimise the detection of FRBs while minimising interference. After tests and validations with pulsars (pulsars are astrophysical objects that emit bursts with properties similar to those of FRBs) and simulations based on the low-frequency FRB model, tools were developed to optimise the process, including weekly observation reports and tests of machine learning algorithms. After several processing campaigns on observations where no FRBs were detected, a more radical optimisation of the pipeline parameters was carried out, allowing the choice of parameters to be adapted according to the type of FRB we were trying to detect. However, even though all the observations have been run through the pipeline several times, it has not yet been possible to look at all the results. So far, no FRB detections have been recorded, but the project has laid a solid foundation for future FRB searches on NenuFAR.

French Summary

Le projet avait pour objectif de rechercher des fast radio bursts (FRBs) en utilisant les données du radiotélescope NenuFAR au sein de l'équipe ASTRO du CNRS d'Orléans. L'étude des FRBs, émissions extragalactiques, ouvre d'importantes perspectives pour acquérir une meilleure compréhension de l'univers qui nous entoure. En raison de l'émergence récente de nouveaux radiotélescopes capables de les détecter, ce phénomène est en expansion. C'est dans cette perspective que ce projet, dont l'objectif est de repérer des FRBs dans des plages de fréquences où elles n'ont jamais été détectées (basses fréquences, de 30 MHz à 80 MHz), a été initié. Une modélisation de FRB a été créée pour représenter leurs caractéristiques physiques et les phénomènes physique qui les caractérisent à ces fréquences. Le développement d'une pipeline était crucial pour gérer les interférences présentes dans les observations du radiotélescope. Cette pipeline a été conçue pour optimiser la détection des FRBs en minimisant les interférences. Après des tests et des validations avec des pulsars (les pulsars étant des objets astrophysiques émettant des bursts ayant des propriétés similaires à celles des FRBs) et des simulations basées sur le modèle des FRBs à basses fréquences, des outils ont été développés pour optimiser le processus, notamment des rapports hebdomadaires d'observations et des essais d'algorithmes d'apprentissage automatique. Suite à plusieurs campagnes de traitement sur les observations sans détection de FRB, une optimisation plus radicale a été réalisée sur les paramètres de la pipeline, permettant d'adapter le choix des paramètres en fonction du type de FRB que l'on cherche à détecter. Cependant, même si toutes les observations ont été traitées plusieurs fois par la pipeline, tous les résultats n'ont pas encore pu être regardés. À ce jour, aucune détection de FRB n'a été enregistrée, mais le projet a établi des bases solides pour les futures recherches de FRB sur NenuFAR.

Contents

List of Figures

List of Tables

Chapter 1

Introduction

This M2 internship consists of searching Fast Radio Bursts using the NenuFAR radiotelescope. The following chapter introduces and presents the environment and the physical concepts needed to understand the issues of the internship and the actions taken to resolve them.

1.1   CNRS and team presentation

The National Centre for Scientific Research in Orleans is a large campus in Orleans that brings together several sectors, including chemistry and physics of materials, environment, propulsion, astrophysics and space, history, economics, biology and biophysics. The team where my internship took place is called the ASTRO team and is part of the Laboratory of Physics and Chemistry of the Environment and Space (LPC2E)[23].

The LPC2E (Figure 1.1) is a scientific research laboratory focusing on three specific areas: Spatial Plasma, Atmospheric and Planetary Environment, and Astrophysics. The laboratory is a joint research unit of the CNRS, the University of Orléans and the CNES and participates in several European missions. Recent reserarch highlights of LPC2E include the launching of the JUICE mission[12].

Figure 1.1: LPC2E main building in Orleans

The ASTRO team is located in the astrophysics branch of the laboratory. Within this team there are five permanent members, two PhD students and one postdoc. During this internship the team grew to 11 people including three internship students. Of these five permanent members, there are Cherry NG, who recently became a CNRS permanent researcher, and Jean-Mathias GRIESSMEIER, an astronomer.

The team works in several fields of astronomy, mainly related to the study of pulsars (see part 1.2.6).

In particular, they study the gamma and radio emission of pulsars. Thanks to these studies, we can derive information about the pulsar itself, for example its rotation period or its magnetosphere. We can also derive information about the wave's path through the cosmos.

A recent publication obtained through the study of its pulsars shows the beginning of evidence for the detection of nanofrequency gravitational waves by studying the periodic emission of pulsars. This had been published at the end of June with the publication of 1the International Pulsar Timing Array (IPTA) [2][3].

1.2 Fast Radio Burst(FRB)

A Fast Radio Burst (FRB) is an electromagnetic burst of astrophysical origin observed in a radio frequency window [17]. We do not currently know the exact origin of the emission of this burst, but we do know that it is an extragalactic burst. Some of them are estimated to be generated several hundreds of millions of light-years away. There are some theories about the possible emission of this one, but they have not yet been verified. Discovered in 2007 by Lorimer[?], this phenomenon is beginning to be studied seriously, as shown in the figure below (1.2)
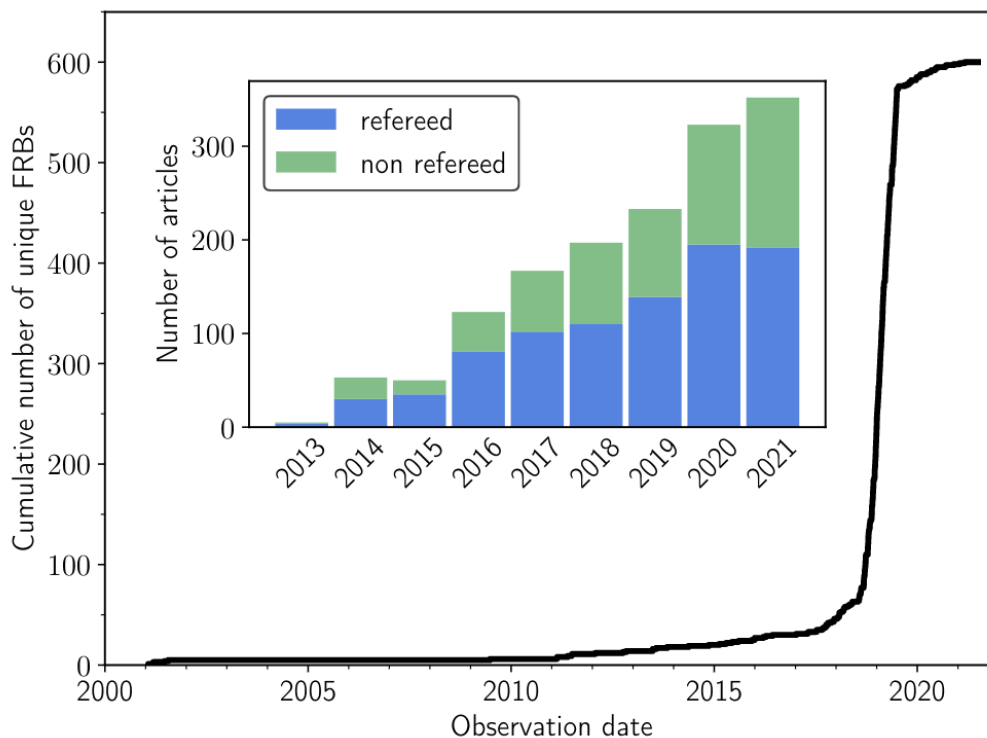
Figure 1.2: Number of unique FRBs found since the first FRB discovery, Credits:Petroff et al. 2022[18]. The x-axis represents the years of discovery and the y-axis represents the number of unique FRBs found.The graph in the middle represents the number of FRB articles published, with the year of publication on the x-axis and the number of articles on the y-axis.This curve is rising sharply because of the increase in FRB discoveries. This has led to an increase in the number of articles on FRBs because of the excitement about the physics behind the study of FRBs. This increase in discoveries is mainly related to the arrival of new radio telescopes.

Figure 1.2 shows that the number of FRB detections has increased significantly since 2019. It is estimated that there could be more than 5,000 FRB bursts per sky per day[15]. Per sky refers

to the fact that a radio telescope can only observe part of the sky, depending on its position on the earth's surface. Moreover, FRBs are relatively bright bursts, it's an electromagnetic wave that is still visible after travelling hundreds of millions of light-years.

FRBs appear as a phenomenon that is observed in large numbers. They are distributed across most of the sky, and have travelled large distances. For cosmological research and for mapping the universe around us, the study of FRBs is a really interesting and new way to get a better and deeper understanding of the universe that surrounds us.

There are several physical effects related to the interaction of the burst with the extragalactic space and the long distances travelled by the burst:

- Dispersion

- Scattering

- Scitillation

- "Sad Trombone Effect"

These effects will be discussed in the following.

1.2.1 Dispersion

For astrophysical bursts transmitted over long distances in the radio wave range, dispersion is one of the phenomena that must be considered because it partially defines the properties of the observed burst[14].

Dispersion, physically represents the interactions of the FRB burst with free elections along the line of sight (1.1). It's an indicator of what the burst has gone through.

$$DM = \int_0^L n_e(l)dl \tag{1.1}$$

which is the integral over the electron density n_e along the line of sight to a pulse at distance L.

On Earth we observe this phenomenon by a non-linear delay between time and frequency. For the same burst, the higher frequency is detected before the lower frequency (see Figure 1.3). It is interpreted according to the following equation (1.2)[14]

$$\Delta T \simeq \mathcal{D} \times (f_1^{-2} - f_2^{-2}) \times DM \tag{1.2}$$

where ΔT is the time delay between 2 frequencies, $\mathcal{D}$ is the dispersion constant defined by equation (1.3), DM is the dispersion measurement related to the studied astrophysical object, f_1 and f_2 are the two frequencies compared.

$$\mathcal{D} \equiv \frac{e^2}{2\pi m_e c} \simeq 4.15 \times 10^3 \text{MHz}^2 \text{pc}^{-1} \text{cm}^3 \text{s} \tag{1.3}$$

where e is the energy of an electron, m its mass and c the speed of light in vacuum.

The phenomenon of dispersion (equation (1.2)) is associated with the frequency of observation and the electron density encountered on the path travelled by the burst.

On Figure 1.3, the effect of burst dispersion is significant. For this low frequency window (40 MHz to 80 MHz), the time delay of the burst from the top of the band to the bottom is about 400 seconds. This is a relatively long time considering that FRB bursts have an emission timescale on the order of a miliseconds. The dispersion measurement (DM) is significant for this value, 349.3 pc.cm^{-3}, but remains within the average order of magnitude for detected FRBs (DM $\sim$ 100 pc.cm^{-3} to 1000 pc.cm^{-3}).
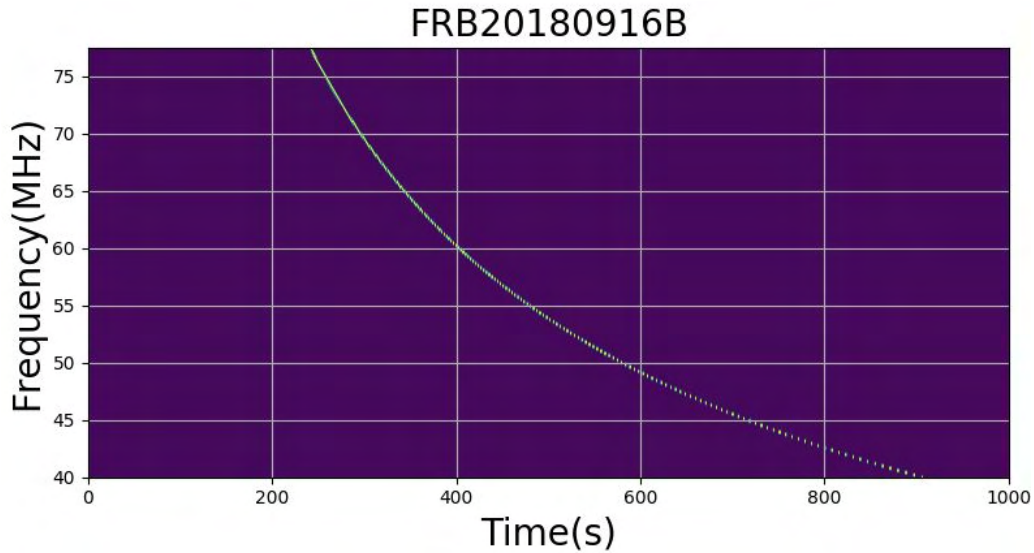
Figure 1.3: Dynamic spectrum of a dispersed FRB burst with a dispersion measure of 349.3 pc.cm^{-3}. This plot is obtained from a model burst, not an observation. The x-axis represents the time in seconds and the y-axis the frequency in MHz. Each point in the dynamic spectrum represents a different frequency channel

DM is related to the distance travelled by the burst, but also to what it encountered along the way. For example, an FRB above the Milky Way will have a smaller dispersion measurement for the same distance travelled than an FRB with an angle of incidence close to the plane of the Milky Way.

To observe this type of burst, it is necessary to dedisperse the observed signals[20]. The idea of dedispersion is to remove the effect of dispersion. We will therefore perform a time shift on the signal frequency according to the value of the time delay introduced by the dispersion phenomenon defined in equation (1.2).

For radio emissions with high DM, if it's not a bright burst, it cannot be detected without this dedispersion.

With this dedispersion, FRB bursts appear as shown in Figure 1.4. In this figure we can see the diversity of the bursts found. In fact, for the same emission sources, the burst can vary in amplitude, but also in its distribution of amplitudes according to frequencies. We can see that without dedispersion we can't get much information about the burst. Dedispersion is necessary to capture the burst, but also to study it.
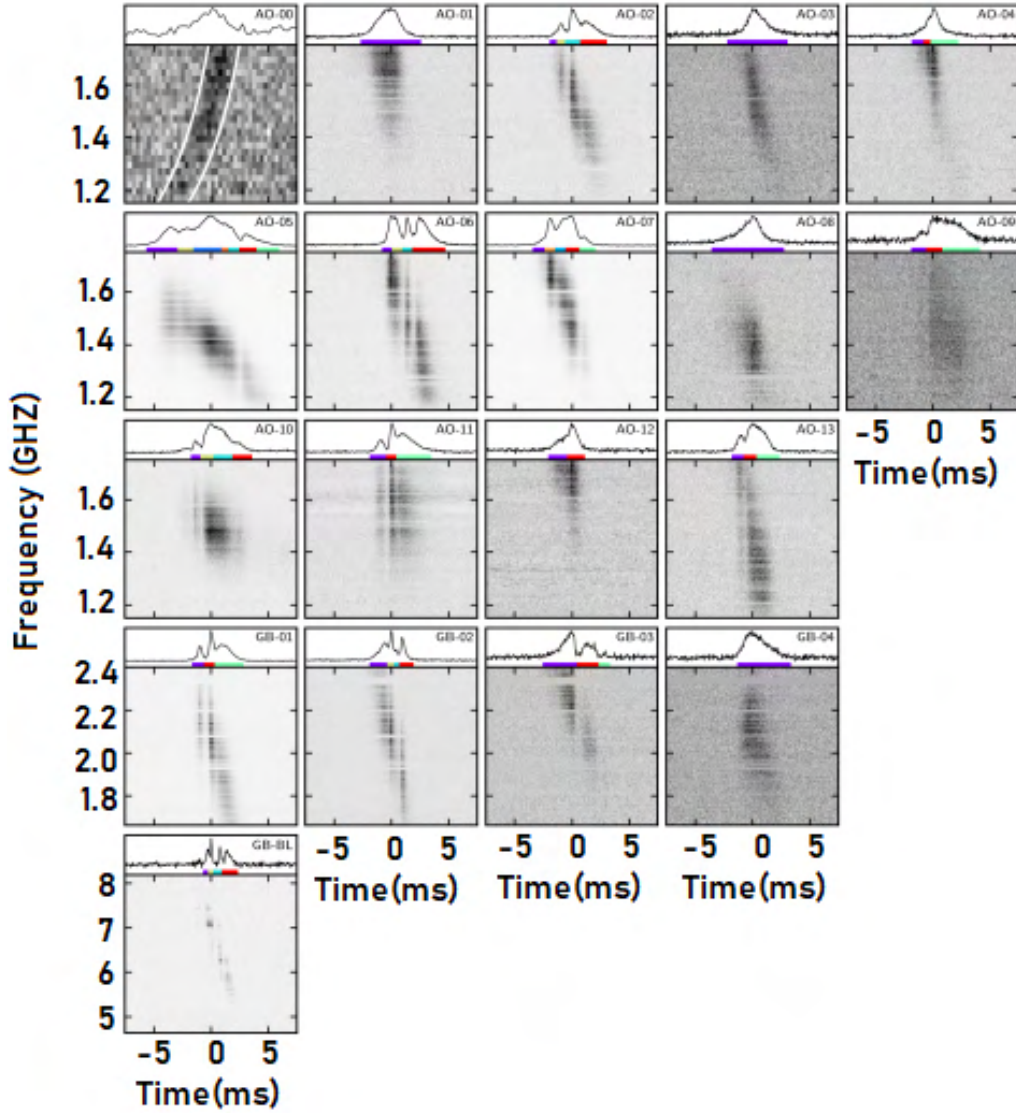
Figure 1.4: Dedisperse dynamic spectrum of different bursts of the same FRB (FRB121102) with different shapes and behaviours. credidts : J. W. T. Hessels et al 2019[11]. Each plot represents the detection of one burst where X is the time in milliseconds and Y is the frequency in GHz. For each burst, we therefore have a dynamic spectrum of the burst with, above, the curve resulting from the frequency integration of the dynamic spectrum.

1.2.2   Scattering

Like dispersion, scattering is related to the distance travelled by the burst[13]. The Fast Radio Burst will pass through clouds of plasma and parts of it will be deflected from its original trajectory. It can then be redirected and travel a greater distance than the undeflected burst. As times goes the burst widens as a function of frequency. The lower the frequency, the wider the pulse is scattered.

The scattering characteristic time represents the burst widening for a given frequency, i.e. the broadening of the FRB burst at the origin around the milisecond. This follows the law given by the equation (1.4). The exponent in the power law varies according to the study and the physical objects examined, but most scientists in the field agree on this value. REFERENCE

$$\tau \propto f^4 \tag{1.4}$$

where τ is characteristic time of the scattering effect and f the frequency.
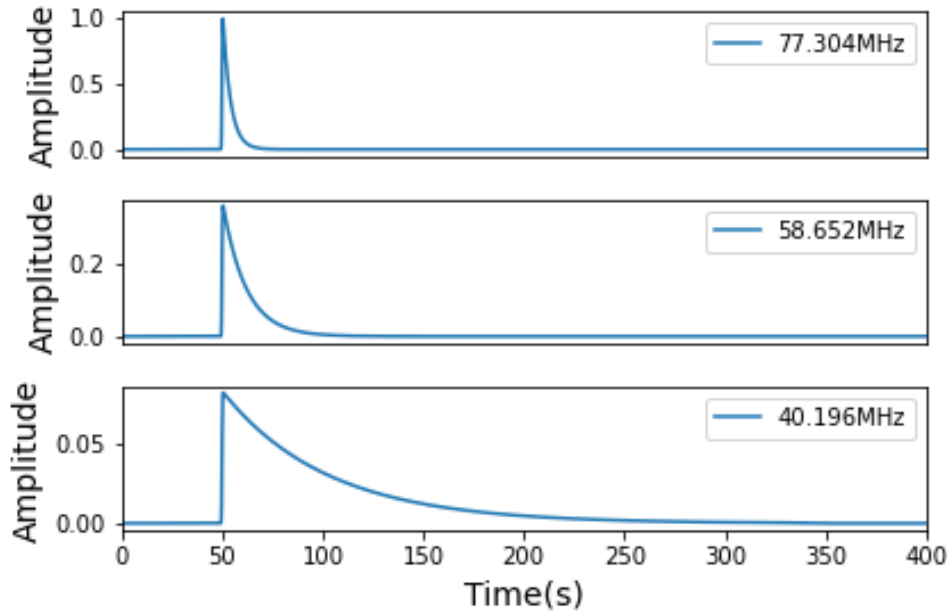
Figure 1.5: Representation of the scattering phenomenon applied for different frequencies. Each plot represents the scattering phenomenon applied to the same burst but at different frequencies. The y-axis shows the amplitude of the scattered signal and the x-axis shows the time in seconds. Each plot, from highest to lowest, represents the frequencies 77.3 MHz, 58.7 MHz and 40.2 MHz.

Applied to the frequencies of interest in the following studies (40 MHz to 80 MHz), Figure 1.5 shows that at low frequencies, the perceived burst no longer has the same appearance as initially. In the same figure (1.5), the initial burst is simulated by a Gaussian with a mean of 200 milliseconds. We can therefore see that the pulse perceived at 40 MHz is more than 150 seconds wide, i.e. more than 750 times its initial width.

By conservation of energy, the longer the scattering has a significant characteristic time, the more the maximum amplitude of the burst will be reduced thus burst amplitudes decrease as frequencies decrease. So it is necessary to take scattering into account when studying distant astrophysical objects.

1.2.3 Scintillation

Scintillation is known from several astronomical sources. It can result, for example from the interaction between the emission source and the ionised Earth's atmosphere. For FRBs observed in the radio range and at long distances, scintillation is related to the interaction with the ionised interstellar medium[16]. The effect of this phenomenon on a burst can be seen by the attenuation or the amplification of the burst in parts of its spectrum. This phenomenon is not considered further, as it is not yet sufficiently important at low frequencies to be compared with dispersion and scattering, but it may be responsible for certain behaviour observed in FRB burst detections.

1.2.4 "Sad Trombone Effect"

This phenomenon, discovered by J. W. T. Hessels [11], is caused by the fact that certain FRBs show a downward frequency drift in their dynamic spectra. That is, after dedispersion of the burst (we have cancelled the dispersion phenomenon, i.e. we have digitally cancelled the time-frequency shift due to the dispersion of the burst), there appears a shift for a certain frequency

(Fig. 1.6). Its name comes from the fact that the output spectrum is visually similar to the sound of a sad trombone. If we integrate the dedispersed dynamic spectrum (top graph of figure(1.6)) in frequency, several peaks appear. Each one represents the amplitude of the burst, but for different frequencies. This phenomenon is interesting because it can give some information about how the burst was emitted.
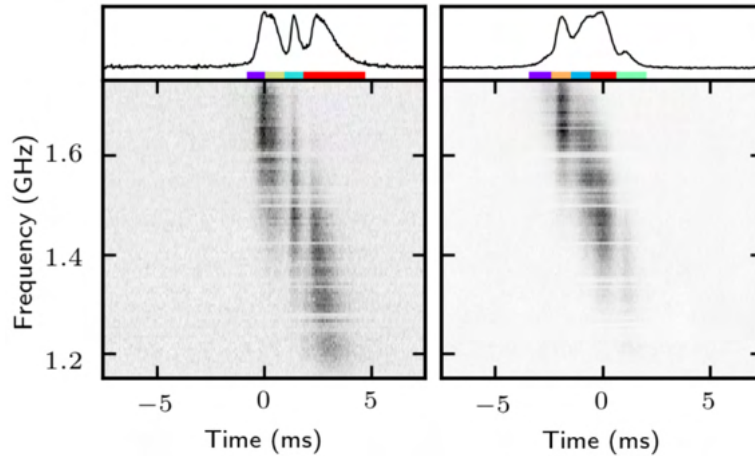
Figure 1.6: Dedisperse dynamic spectrum of an FRB with a strong downward frequency drift. credits : J. W. T. Hessels et al 2019 [11]. X-axis : Time in millisecond Y-axis: Frequency in Gigahertz. On the top of this figure, it's an frequency integration plot to see the amplitude distribution. Bottom plots: dynamic spectra

The previous four subsections give an idea of the physics applied to FRBs during their journey to Earth. The next subsection introduces on another peculiarity of FRBs.

1.2.5 Repeating FRB source

Over the past decade, astronomers have made numerous discoveries of FRBs. More than 600 sources have been identified to date [18]. However, most of these FRBs have been non-repeating, showing a single burst event. Only a small fraction of FRBs have been observed to repeat. As a result, astronomers are now asking questions about the origins of repeating and non-repeating FRBs.

Repeating FRBs are special because their repetition is dictated by two states, an active state and a inactive state[10]. During the active state one or more bursts can be detected. During the passive state, the source appears to be switched off. These on/off states are unique to each repetitive FRB. The example of FRB20180916B is relevant to explain this phenomenon. It has an activity period of four days and then is in an off state for 12 days.

There is another phenomenon specific to FRBs that is currently only demonstrated for some repetitive FRBs. It is not yet known whether this applies to all repetitive FRBs and whether it also affects non-repetitive FRBs. This effect is called the delay window[19]. This refers to the fact that an FRB burst can be seen at around 600 MHz (the centre frequency of the CHIME radio telescope) and appears at around 150 MHz with a significant time delay. In the case of FRB20180916 this delay is about 3 days. This is unreleated with the dispersion phenomenon explained above.

1.2.6 Pulsar

Pulsars are the Astro Team's main astrophysical objects. We therefore have a detailed knowledge of their location and how they are detected. Pulsars are extremely dense neutron stars

with fast rotation periods (ranging from milliseconds to seconds). There are several types of pulsars, such as those that emit in the X-, gamma- or radio-domain. For our purposes we are only interested in the radio range. The distance of a pulsar affect the DM and the scattering, which for most pulsars will be much smaller than for FRBs. The pulsar's pulse will then be much easier to detect because it is less dispersed in time and the dispersion for some of them are well know. It's the same with scattering. For comparison, an FRB (FRB180916) at 600MHz will have a characteristic scattering time of 1.05ms, while the pulsar (B0329+54) will have one nanosecond. For the dispersion measurement we will have a DM of 350 pc.cm^{-3} for the FRB and pc.cm^{-3} for the pulsar. So we have different orders of magnitude. It's interesting to begin the first analyses on pulsars because they undergo the same physical phenomena resulting from the interaction of the burst with the interstellar medium. In addition, pulsars have a constant and periodic emission. We know that if we point the telescope at the coordinates of the pulsar, the burst will be detectable. This is useful when we are trying to calibrate a pipeline to detect FRBs.(See 3)

To detect radio waves, you need tools to detect them. The following section introduces the concept required for their detection.

1.3   Radioastronomy

Radio astronomy is a branch of astronomy dedicated to the study of radio waves, i.e. any signal coming from the sky with a frequency ranging from tens of hertz to hundreds of gigahertz. For an electromagnetic wave coming from space, radio astronomy is concerned with a wave with a wavelength between 100000 kilo-metres and one micro-metre.
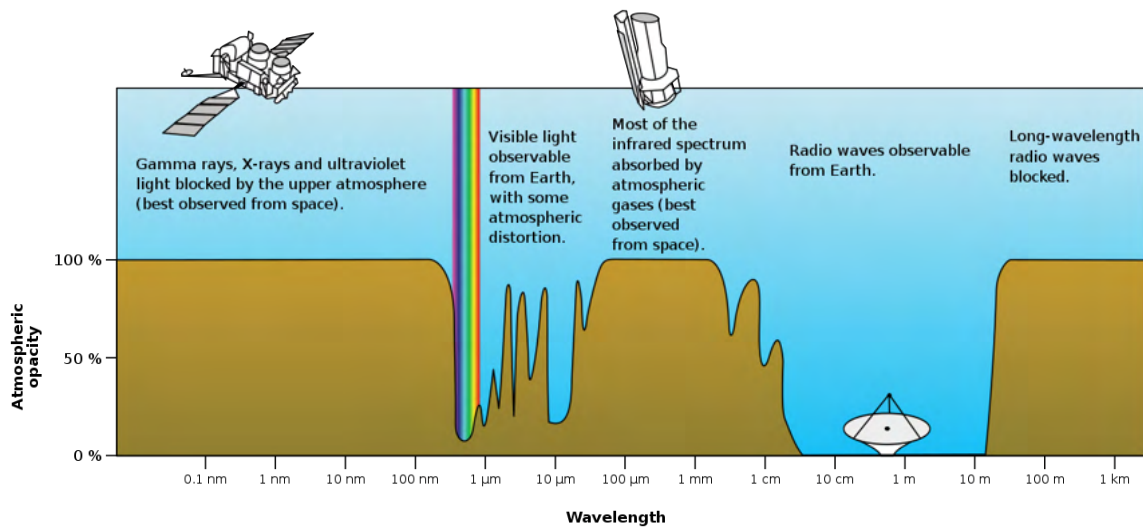
Figure 1.7: Graph of wavelengths captured by the ionosphere, Credits: NASA. On the x-axis we can see the wavelengths, and on the y-axis the percentage of waves of that wavelength that are captured or reflected by the ionosphere.

Fig 1.7 shows that the atmosphere, and the ionosphere, does not allow all frequencies to reach the Earth's surface. For radio waves, all waves below 3 MHz (wavelength greater than 100m) are not observable from the ground, and the same applies to waves above 30 GHz (wavelength less than 1cm). So the frequency range between (3 MHz and 30 GHz) is interesting, because these waves can be observed from the ground. Ground-based radio telescopes are therefore very useful for studying waves in this frequency range. Because they are easier to set

up and more flexible than satellites, a large telescope will have greater sensitivity than satellite, so observing the sky in this frequency range is relatively easy to set up.

1.3.1 NenuFAR Radiotelescope

There are several radio telescopes that detect FRBs. CHIME, the Canadian radio telescope, and FAST, the Chinese radio telescope, are the two telescopes currently detecting the most FRBs. In Europe, the Nancay Observatory[22], south-east of Orléans, is an important point in internatioal. It comprises five different radio telescopes: The NRT (Nançay Radio Astronomy Observatory) observes in the 1.0 to 3.5 GHz band and is the fourth largest in the world in terms of collecting area. It receives electromagnetic waves from the universe and observes mainly galaxies and extragalactic signals. LOFAR, a European interferometer[4], is shown in Figure 1.8a It has one of its stations at Nançay. It observes the sky at low frequencies (110 MHz to 270 MHz) and compares the results from all these European centres to increase its sensitivity. NenuFAR (New Extension in Nançay Upgrading LOFAR) was originally conceived as an extension of LOFAR for lower frequencies than those currently used. It has been operational since 2019. There are also two other sets of antennas for observing the Sun and Jupiter.
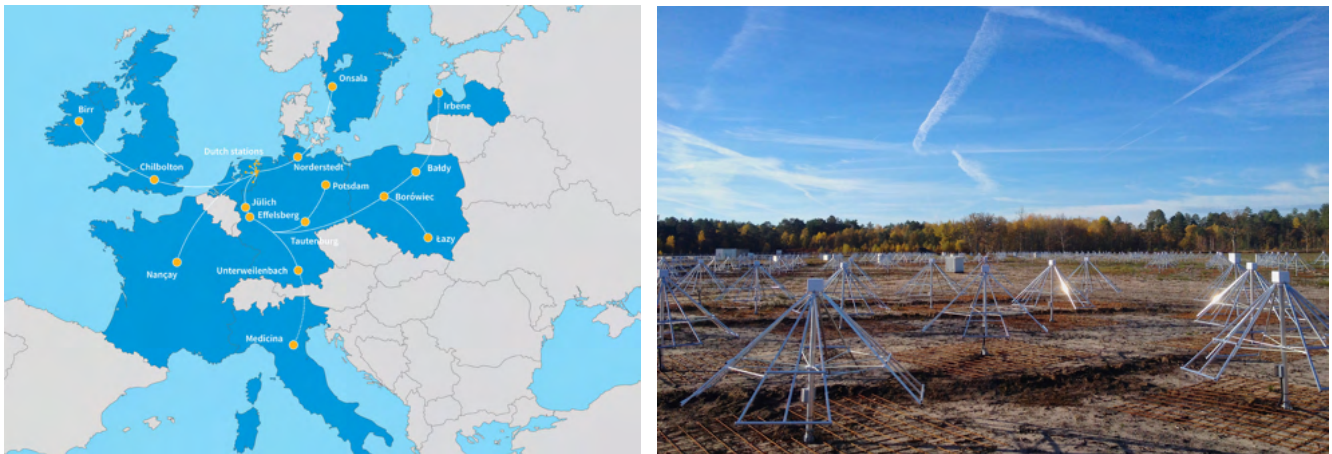
(a) Illustration of the LOFAR interferometer along with all its installations throughout Europe[4].

(b) Photograph of NenuFAR in Nançay, illustrating the shape and alignment of the radio telescope's antennae. credit : Nenufar[22].

Figure 1.8: NenuFAR and LOFAR seen in image. The illustration on the left depicts LOFAR's disposition, while the image on the right shows the radiotelescope NenuFAR.

NENUFAR is innovative and physically interesting because it observes between 10MHz and 80MHz, a frequency range that has been little used in celestial research due to the presence of a large number of satellites. Frequency range that has been little used in astronomical research due to the presence of a large number of interferences. Interference (see 2.2). Nenufar has the peculiarity of having a large number of antennas, as shown in Fig. 1.8b (more than 90 groups of 19 antennas placed in a circle 400m in diameter), which makes it one of the most sensitive of the existing radio telescopes in this frequency window, and thus able to see and detect astrophysical stars. This internship is be based on the data recovered by NenuFAR (Backend telescope by L.Bondonneau[5]).

Chapter 2

Internship objectives

The current excitement about FRBs, the interest in studying the universe around us, and the fact that no FRBs have been detected in the NenuFAR frequency band so far, gives real interest and motivation to carry out this internship. The aim will then be to find a way to detect FRBs with all the difficulties that low frequencies can bring. The study will be divided into three main sections. A section on the analysis of the database provided by the NenuFAR observations. Making an inventory of the existing observations; understanding which source of FRBs is interesting, which observations could be interesting, and understanding the impact of RFI, the big problem at low frequencies. The second part (see section (3)) will be entirely devoted to setting up the pipeline needed to process the observations and optimising this pipeline. Finally, (see section (4)) the last part will be devoted to studying the signal present in the observations and searching for FRBs in the observations.

2.1 Prior Insights: Framing the Context

Since its creation in July 2019, NenuFAR has been recording parts of the sky, and some of its observations are deliberately aimed at some FRB source positions. These observations are therefore present in the database, but have never processed. The observation is then in its original state at the output of the radio telescope.

Figure 2.1 shows the distribution of all the FRB observations that have been made by NenuFAR. Each FRB source is defined by the acronym FRB, followed by its original discovery date. The letter after the discovery date makes it possible to distinguish two FRB sources discovered on the same day. The SGR stands for Soft Gamma Repeater and is used because it behaves like an FRB. The zenith is also present and represents a pointing test in the sky . Most of them are periodic FRB sources (see section 1.2.5). They are interesting astro-physical objects from a first detection point of view because we know their characteristics quite well. They are often observed at high frequencies. All the information and precision can be found in Table 2.1 as observed by CHIME. CHIME is a Canadian radio telescope that has found and detected a large number of FRBs between 400 MHz and 800 MHz, it's currently one of the most active telescopes in terms of FRB detections.
The characteristics used to distinguish and interpret an FRB are the source coordinates, as they allow the telescope to define a direction. These data are not included in the table as they are not of interest for this signal analysis study. On the other hand, for an FRB detection, the parameters intrinsic to the FRB signal are necessary and are presented in each column of the table 2.1. The dispersion measure (DM) represents the dispersion (eq. (1.3)) of the burst and is defined in pc.cm^{-3}. The parsec (pc) is a unit of length used to measure the large distances to astronomical objects outside the solar system, about 3.26 light years. The fluence, which
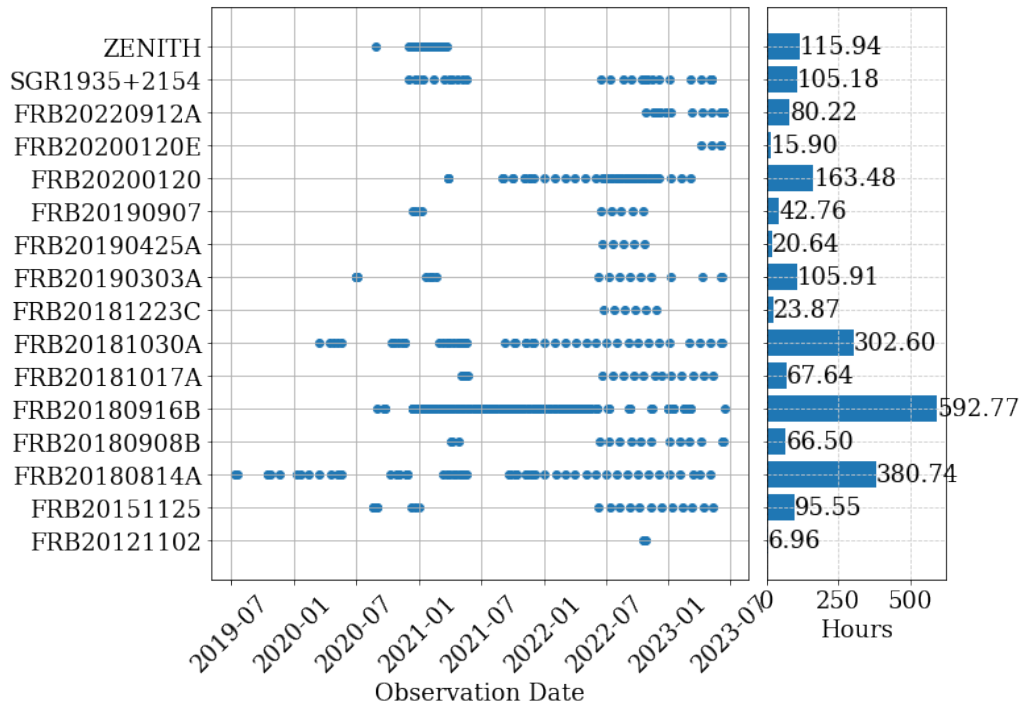
Figure 2.1: [Temporal plots of FRB observations made with the NenuFAR radio telescope. In the main plot, the x-axis represents the dates of the different observations, sorted in chronological order. On the y-axis we find the names of the observed astronomical objects, FRBs, but also an SGR (soft gamma repeater). On the right, the graph represents the cumulative observation times of each observed astronomical object. On the x-axis is the cumulative time in hours and on the y-axis is the name of the astronomical object.

determines the energy of the burst detected or the intensity of the flux over a period of time, is important. It is defined in Jy.ms. The Jansky, symbol Jy, is the unit commonly used in radio astronomy to measure the signal intensity, or more precisely the flux density of radio signals. A jansky is defined as a flux of 10^{-26} watts per square metre of reception area and per hertz of bandwidth ($1\ \mathrm{Jy} = 10^{-26}.\mathrm{W}.\ \mathrm{m}^{-2}.\mathrm{Hz}^{-1}$)

The characteristic time for scattering, section 1.2.2), at 600 MHz determines a characteristic time for the scattering burst detected at 600 MHz (by Chime [7]). This value can then be used to obtain the theoretical scattering for other frequencies according to the power relation of this scattering characteristic time eq. (??ch observation lasts 4 hours and is preceded by an hour of observation on Pulsar to calibrate the instrument. This allows us to know if the FRB observation might be disturbed by radio interference or other unusual phenomena like bad radio telescope pointing, sky noise etc.

FRBs name	DM (pc.cm^{-3})	Fluence (Jy.ms)	Scattering time at 600MHz(ms)
FRB20180916B	349.3491±0.0058	6.1±1.7	0.105
FRB20200120E	87.7527	2	0.23
FRB20181031A	103.396±0.0058	8.2±5.9	0.88
FRB20180814A	189.286±0.076	2.6±1.0	3.1
FRB20180908B	195.239±0.0064	5.0±1.7	2.1
FRB20220912A	218.9±0.8	65	None
FRB20190303A	221.667±0.017	2.54±0.97	2.96
FRB20181017A	239.97	13-52	∼0.00158
FRB20151125	273	2450	None
FRB20190907	310.9	1.7	None
FRB20121102A	564.367±0.043	12.6±5.5	6.9
SGR1935+2154	332.7	112.3	∼0.759
FRB20190425A	128.15774±0.00016	31.6±4.2	∼0.38
FRB20181223C	112.5118±0.0035	2.84±0.93	∼0.107

Table 2.1: Information about all FRBs observed by nenuFAR. Each column defines a characteristic.
Col1: FRB name, Col2: DM in pc.cm^{-3}, Col3: Fluence in Jy.ms, Col4: Scattering time observed for this FRB at 600MHz.

Most of them are repeaters, except the last two on 2.1 Table. Repeating FRBs are interesting because we know that the source we are looking at can emit again. Nenufar has a little more than 200 different observations spread over 10 different FRB sources, Figure (2.1) shows that the distribution is not identical between them. It will therefore be necessary to make choices to select the relevant observations i.e. observations where we can hope to find something to explore them more specifically ! The study of the noise present in observations, also known as Radio Frequency Interference, can also be decisive. If an observation is too noisy, it may beacame impossible to extract the information it contains.

2.2 RFI Challenge

Radio Frequency Interference refers emission of radio frequency energy that caused by an electronic or electrical device to generate disturbing noise that can interfere with the proper functioning the telescope, and the RFI appears as energy spikes that contaminate the radio signal. In general, most of the RFI is associated with human activity and increases significantly during the day.

Fig 2.2 shows all the bright RFIs that can be observed on Nenufar's FRB observations. It's important to note that the day observations are very bright compared to the night observations. There are different teams on NenuFAR and they all want something without RFI, so the night slots are more valuable and more booked than a day slot. For NenuFAR, night hours are defined for observations between 6 p.m. and 4 a.m. In our case, with 4 hours per observation and 1
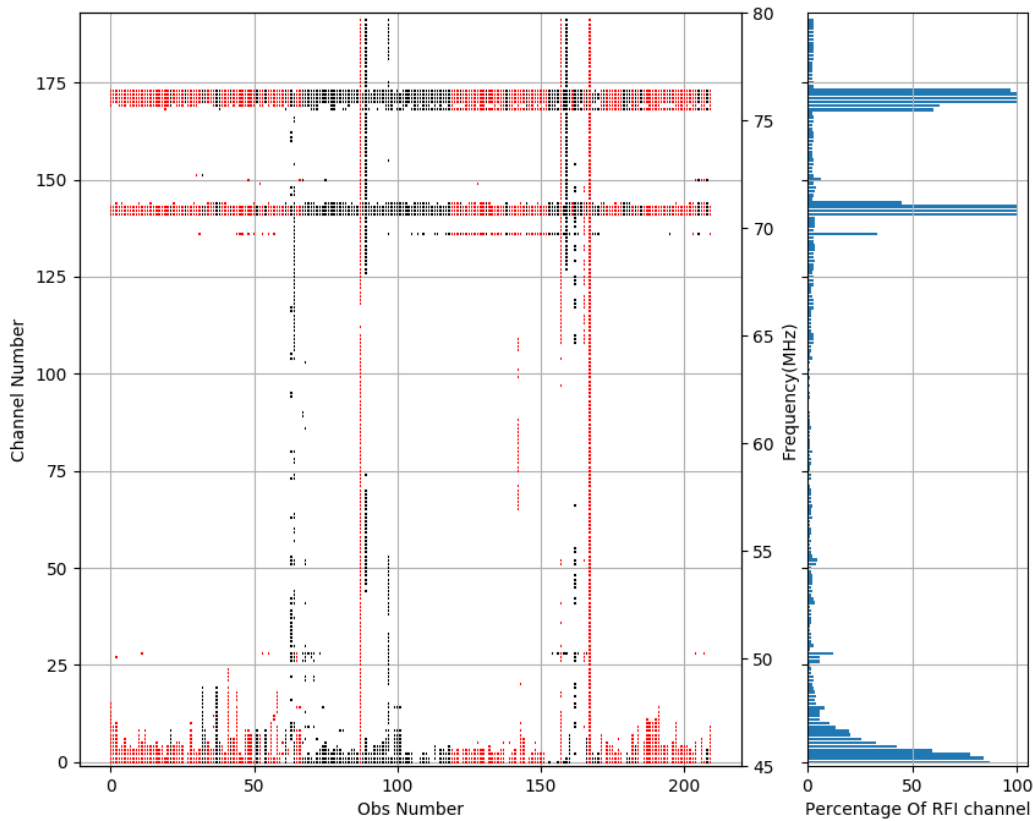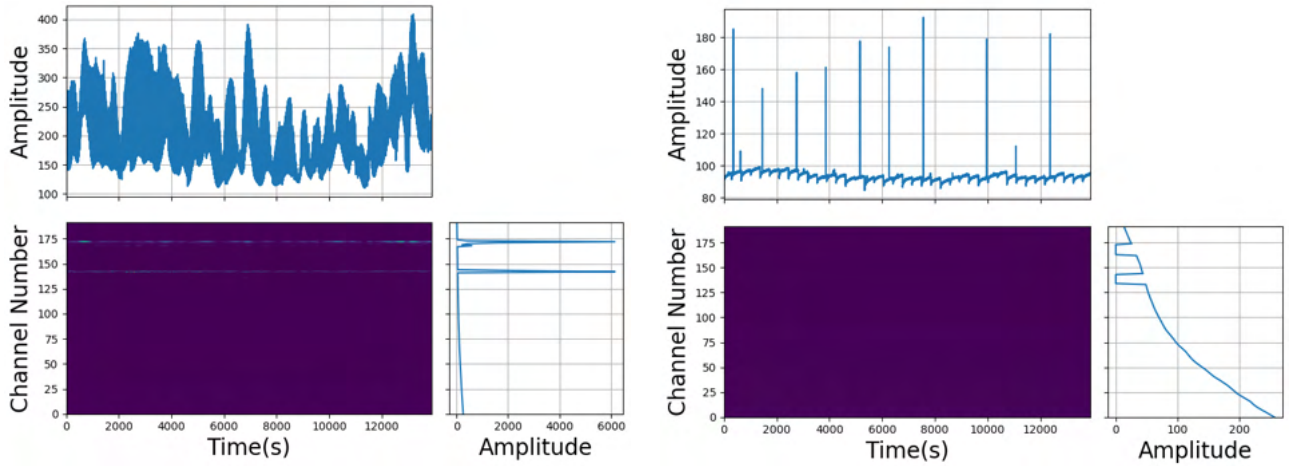
Figure 2.2: Radio frequency interference plot of FRB observations by NenuFAR. There are two graphs, on the left, the X-axis represents the number of observations in chronological order and the Y-axis represents the number of frequency channels on the left and the corresponding frequencies on the right. Each point represents one perturbation. Black represents night observations and red represents day observations. The plot on the right represents the percentage of RFI on the FRB NenuFAR observations, in X we find the percentage of presence of the RFI, in Y the corresponding frequencies.

hour before for pulsar calibration, booking one of them is very complicated. It's mainly for this reason that most of the FRB NenuFAR observations are in the daytime range, the red colour in Figure 2.2 compared to the dark colour for the nightime observation.

The lower part of the figure 2.2, below 47 MHz, is very bright, corresponding to the fact that the energy of the average sky increases at low frequencies. It's not interference, it's just greater average energy. A normalisation of these signals will help to avoid this phenomenon.

Looking at the other visible interferences, we can see that some frequency channels are always saturated.For ewample, around 77 MHz or around 72 MHz. It is then necessary to deal with these important interferences. Also some observations are completely noisy. It is necessary to avoid working with these particular observations.

Figure 2.3a shows an unprocessed observation with all its RFI. The frequency integration of the signal at the top of the figure shows that there is a significant variation in the baseline of the signal as well as a significant variation in the integrated energy (between 150 and 200 units). There is a lot of noise. The right side of Figure **??**, represents the time integration that made it possible to detect the frequency RFI and to produce the figure 2.2 when we apply it to all the observations.. We can clearly see the presence of RFI for certain frequencies. Figure 2.3b is the same observation with the frequency channels with justified RFI removed by thresholding . It can be seen that the dynamic spectrum of the observation, the main image, no longer has an obvious bright spot, i.e. a bright RFI. In addition, the baseline is more stable and the variation between them is greatly reduced (90 and 180 units). In this particular case we have

(a) Dynamic spectrum of an unprocessed observation

(b) Dynamic spectrum of an unprocessed observation without frequency interference

Figure 2.3: Two plots each representing an observation of FRB made by NenuFAR with no treatment on the left and a treatment on frequency RFIs on the right. Each of the two plots happens to be a dynamic spectrum with times in seconds in x and frequencies in MHz in y. At the top of each dynamic spectrum we find the frequency integration plot with in X the time in seconds and in Y the amplitude of the signal and on the right the time integration plot with in X the amplitudes and in Y the channel number.

not touched the local RFI (over a short time interval) but only the frequency one, so there is still some processing to do to properly process the signal, but this first approach shows the importance of removing the RFI to detect possible FRBs.

2.3   Interest of repeating FRB

The last thing to consider is where to look for FRBs. We have more than 200 observations of more than 4 hours, or more than 800 hours of observations, spread over 10 different FRB sources. So the idea is to look at the repeating FRBs to know where to start i.e to know a position, a DM and a scattering characteristic time, but also to compare with radio telescopes that look at higher frequencies and detect repeating FRBs. We can then define interesting and active FRBs, but also observations that may contain an FRB detected by another telescope. We therefore compared the observations of NenuFAR with those of the two most powerful radio telescopes in terms of FRB detection, namely the Chime radio telescope mentioned above and FAST, the new Chinese radio telescope. Both radio telescopes operate at higher frequencies than NenuFAR.

   We find two FRBs that are really interesting in terms of activity. The really active one FRB20180916B and the recently discovered FRB20220912A, which is really active recently. A comparison between NenuFAR observations and chime detections of FRB201800916B since NenuFAR measurements began has been made. Fig 2.4 plots the observations of NenuFAR and the detections of CHIME on FRB201800916B[8], the blue points represent the observations of NenuFAR according to the dates of the CHIME detections (in X). Each point is on a scale of + or - 8 days (in Y) around the detection date. The red zone represents the previously defined activity window (section 1.2.5) (3.6 days for this FRB) and the green zone the delay window (section 1.2.5) (3 days between the CHIME and NenuFAR frequencies for this FRB). Theoretically, the observations in the delay window of each CHIME detection could contain the FRBs detected by CHIME. They are therefore interesting to study in more detail. Fig.

2.5 compare the detections of CHIME and FAST on FRB20221912A[21], the crosses for the observations compared to FAST and the dots for those compared to CHIME. we do not have much knowledge about the delay window of FRB20220912A, but we still observe a good number of connections where NenuFAR observations are close to FRB detections from other telescopes . It can be noted that the latest CHIME detections are from July 2023, and so we have made some observations around this detection date in the hope of finding something. We can therefore note a number of potentially interesting NenuFAR observations priority for data analysis.
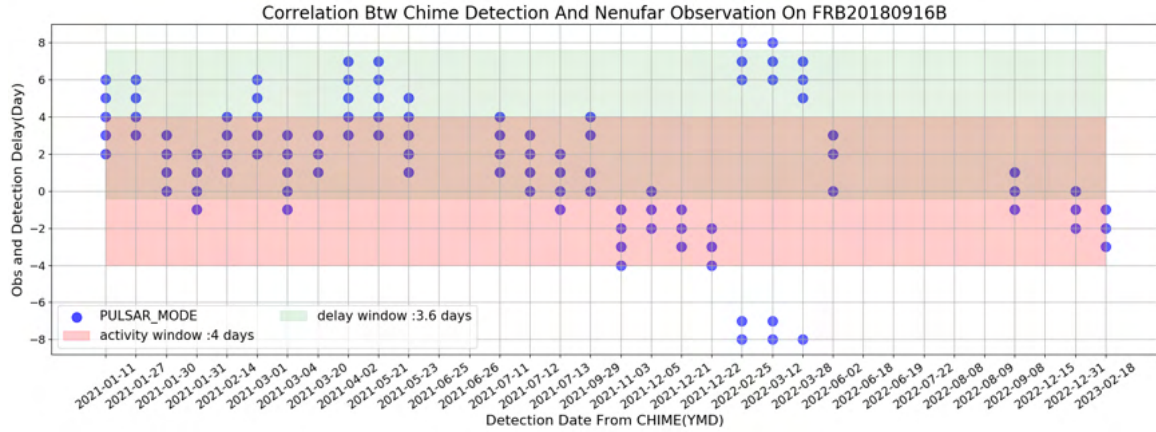
Figure 2.4: A plot showing the possible links between the NenuFAR observations and the CHIME detections of FRB20180916B.Each point represents an observation of NenuFAR. They are compared with the detection date of CHIME on the same FRB, which defines the X axis. The Y axis defines the difference in days between the detection and the NenuFAR observations. 0 represents a detection and an observation on the same day. -1 indicates that the observation took place the day before the detection and 1 the day after.
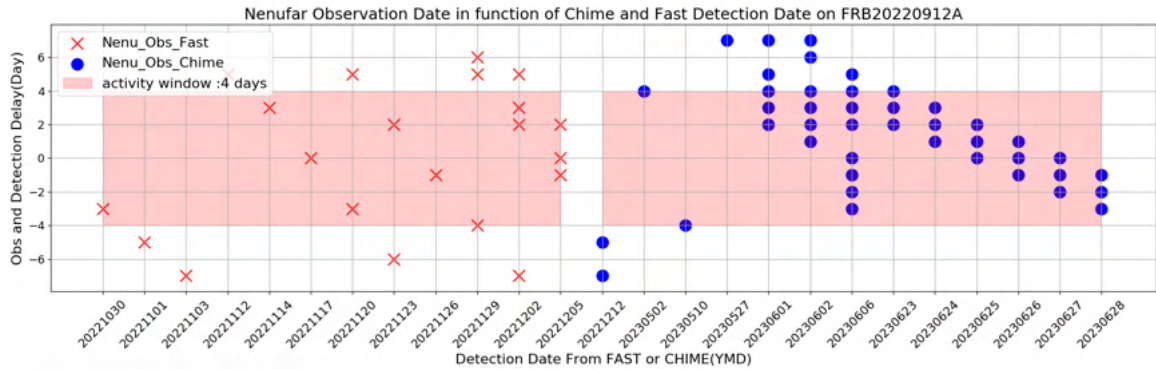
Figure 2.5: A plot showing the possible links between the NenuFAR observations and the CHIME and FAST detections of FRB20220912A. Each dot represents an observation of NenuFAR. The cross is for the comparison between FAST and NenuFAR and the circle is for the comparison between CHIME and NenuFAR. They are compared with the date of the CHIME and FAST detections on the same FRB, which defines the X axis. The Y axis defines the difference in days between the detection and the NenuFAR observations. 0 represents a detection and an observation on the same day. -1 indicates that the observation took place the day before the detection and 1 the day after.

The second interesting point about repetitive FRBs is that we know the dispersion measure of the FRB. We can then apply coherent dedispersion. The radio telescope acquires 37.5 MHz of bands between 42.5 MHz and 80 MHz. After digitisation, 192 frequency channels with a

frequency step of 195 KHz per channel. On the other hand, there are more channels at the time of recording. The frequency step is much smaller, but they are then compressed to reduce the size of the observation backup. The interest of coherent dedispersion is to electronically dedispersing the interior of each of the 192 future channels and then creating a dedispersed signal to the known DM of the FRB source. This is called intra-channel dedispersion.
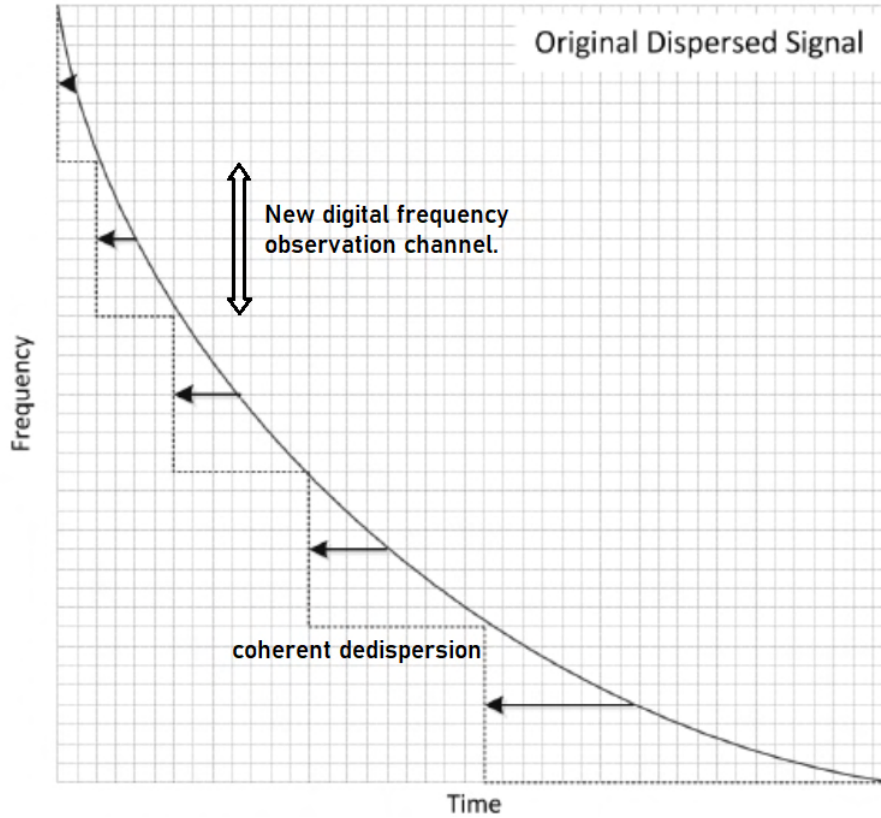
Figure 2.6: Diagram of coherent intrachannel dispersion, The x axis shows the time, the y axis the frequencies, the curve in the background are the representation of an unsampled burst (in real time).

Figure 2.6 is a diagram showing how coherent desdispertion works. As each channel is already dedispered before the numerical study of the observation, the dedispersion action to detect bursts can only be more precise. The only drawback is that you need to know the precise DM of the source you want to look at.

Chapter 3

Results

In the previous part we introduced the concepts, the physical aspects and the decisions necessary to achieve the goal of the internship, namely to search for Fast Radio Bursts on NenuFAR. We have two candidates as active FRBs, FRB20180916B and FRB20220912A. The main focus will be on these FRBs. The main goal of this M2 internship is to process the data in an automatic and efficient way in order to extract the information it contains. This leads to the creation of a pipeline to process the observations. The idea is to create a single script capable of processing everything in the same way and to optimise this pipeline.

3.1 Pipeline

According to the previous section, the pipeline must meet several criteria in order to work as a signal processing and RFI removal system. The pipeline must perform three main actions: catch RFI, dedisperse the dynamic spectrum and detect or not the presence of an FRB.

Figure 3.1 shows the pipeline that will be used to process the observations. It is inspired by the PRESTO pipeline[24] used to process pulsars and the work of Marc Brionne.(Mark Brionne is a recently graduated PhD student in the ASTRO team[6]). This pipeline can be divided into four different parts, the inputs, the outputs, the signal processing part and the detection part. The input is a dynamic spectrum of an observation (Fig. 3.2a). For certain tests, a simulation of an FRB is added (see 3.3). The other inputs are the parameters of the scripts present in the pipeline. The output is a DM (dispersion measure) vs time plot, which allows to directly determine whether an FRB is present or not (Fig. 3.17). There are also some files that allow a machine learning algorithm to process the data automatically. The signal processing part aims to process the RFI, but also to normalise and flatten the signal to reduce the effect of the radio telescope gain. The detection part aims to dedisperse the signal and apply detection algorithms to determine the presence or absence of FRBs. The parts of the pipeline explained in the following subsections.
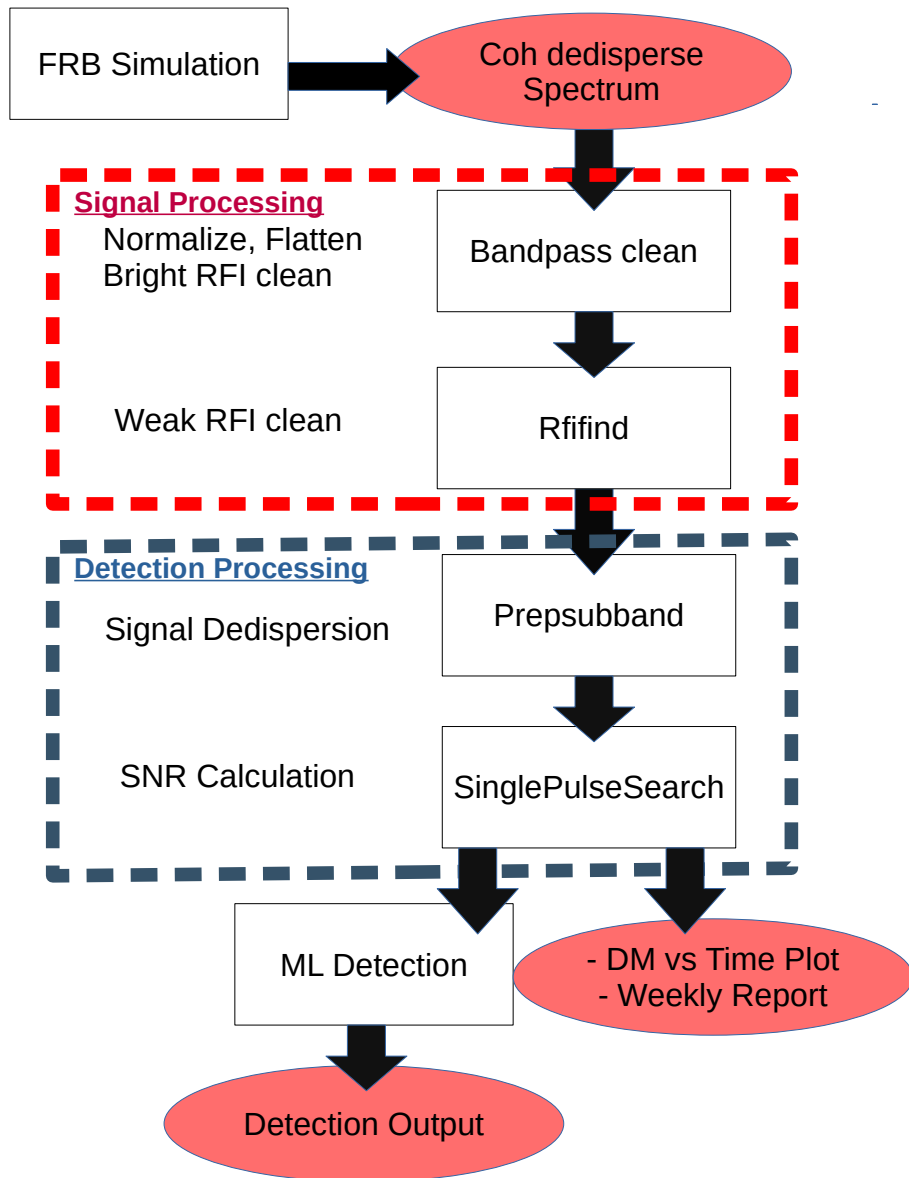
Figure 3.1: Diagram of the pipeline used to process NenuFAR observations. Each block representing a different script.

3.1.1   Signal Processing

As for the input to the pipeline, we have a coherent dedispersed observation. Figure 3.2a shows the type of observation made by NenuFAR. As before, the figure shows the dynamic spectrum of the observation made, in this case for FRB20180916B, with a frequency-integrated time signal from the dynamic spectrum at the top of the figure and a time-integrated frequency representation on the right of the figure. We will process this signal using two scripts, described in the two sections below.

Bandpass clean
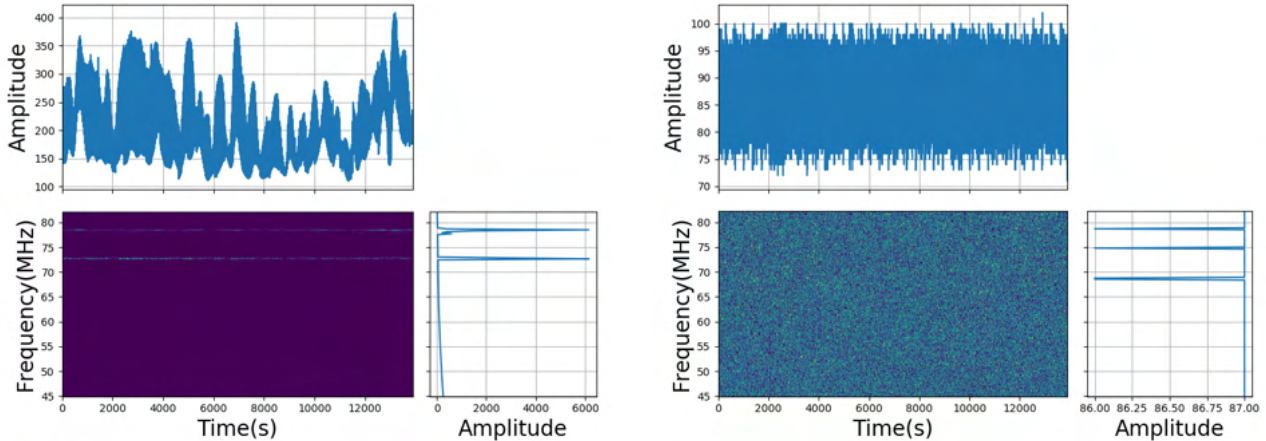
(a) An observation from FRB20180916B not processed

(b) An observation of FRB20180916B processed by the 'bandpass' script

Figure 3.2: Two plots are shown, each representing an observation of a Fast Radio Burst (FRB) made by NenuFAR, with no treatment on the left and with a 'bandpass script' treatment on the right. Each plot is a dynamic spectrum, with seconds on the x-axis and frequencies in MHz on the y-axis. At the top we see the frequency integration plot, with seconds on the X-axis and the amplitude of the signal on the Y-axis. On the right is the frequency integration plot, with amplitudes on the X-axis and frequencies in MHz on the Y-axis.

Written mainly by Louis Bondenneau[5], this script makes many modifications to the observation. The observation was first converted to a special format. These are many arrays of 512 by 192. 512 time channels and 192 frequency channels. To this we add 4 polarisations for each array. Physically, one frequency channel represents 192 kHz and one time channel represents 0.0209 seconds. This is defined by the transition from analogue to digital observation of the telescope. Each array therefore originally represents a block of 10.7 seconds and 37.5 MHz. For four hours of observation, we therefore have more than 1370 arrays making up the signal. This type of segmentation is interesting because it defines the blocks on which we will statistically remove radio frequency interference. This script therefore first reformats the observation blocks to the desired block size. It then suppresses the four polarisations (crunch) to leave only the absolute amplitude of the signal, which is necessary for detection. The large RFI is replaced by Gaussian noise according to the observation statistics. Bright RFI is detected by applying a threshold to the mean and standard deviation of each block of the observation. The script converts the observation from 32 bits to 8 bits to optimise the observation for further processing. Finally, the last part of the script flattens the signal to avoid introducing biases related to sky strength (time variation) or telescope bandwidth (frequency variation). This is done by subtracting the mean from each time block and dividing by the median absolute deviation. Figure

3.2b shows the results of the script applied to the signal of figure 3.2a. The time-integrated and frequency-integrated signals have been flattened, eliminating temporal variations. We can also see a reduction in the impact of low frequencies on the overall energy of the signal i.e all frequency channels have the same average energy. The script also mask out frequency channel around 73 and 77 MHz to zap RFI.

This raises the question of whether the signal processing is destructive. However, it should be that any FRB burst will be spread over a period of more than 300 seconds and will be scattered over a few seconds. Thus the pulse will appear on many time channels. The loss of information due to the script does not have a significant effect on the signal quality. The size of the blocks defining the format of the observations made during the first stage of this script will then be an important choice when considering the processing of the observation and will be discussed in the pipeline optimisation section.

Rfifind

Having looked at the shape of the signal, it is necessary to look at low-amplitude RFI. An RFI processing algorithm is then required, RFIFIND. This algorithm is often used to find RFI in pulsars (PRESTO pipeline[24]). The interest is to optimise these parameters so that only the RFI is destroyed and not the FRB burst.

The algorithm takes an observation as input and returns a mask that defines the frequency-time coordinates to be ignored in the observation. There are three types of processing performed by RFIFIND.

Figure 3.3 shows the RFI mask created by RFIFIND. The plot at the left represents the first processing. It processes periodic RFI. It is a Fourier transform filtering applied to each signal block defined by the 'bandpass' script. They are defined in red. The two rectangles in the middle represent the temporal RFI processing. Thresholds are applied to the signal blocks on the left and to the mean of the signal blocks on the right. The RFI is shown in green for the unaveraged signal and in blue for the averaged signal. Finally, the rectangle on the right represents the sum of the three treatments and therefore the output mask. There are four parameters that can be used to optimise the processing of this script : two thresholds (time and frequency standard deviation), the frequency threshold (SigmaF) and the time threshold (SigmaT), which define the thresholds for the three processes (previous rectangles). Two ratios, a time ratio (BerrT) and a frequency ratio (BerrF), which define whether a time channel or a frequency channel is retained or not. For example, if we set BerrF to 50% and RFIFIND finds that more than 50% of the points for this frequency are RFI, then all the channels will be considered as RFI.

Finally, it's important not to push the parameters too far at the risk of destroying any FRB bursts. Figure 3.4 shows that for a simulated burst, if you're not careful, you could find that our simulation is considered as RFI. The destroyed burst is shown in the blue rectangle in Figure 3.4.
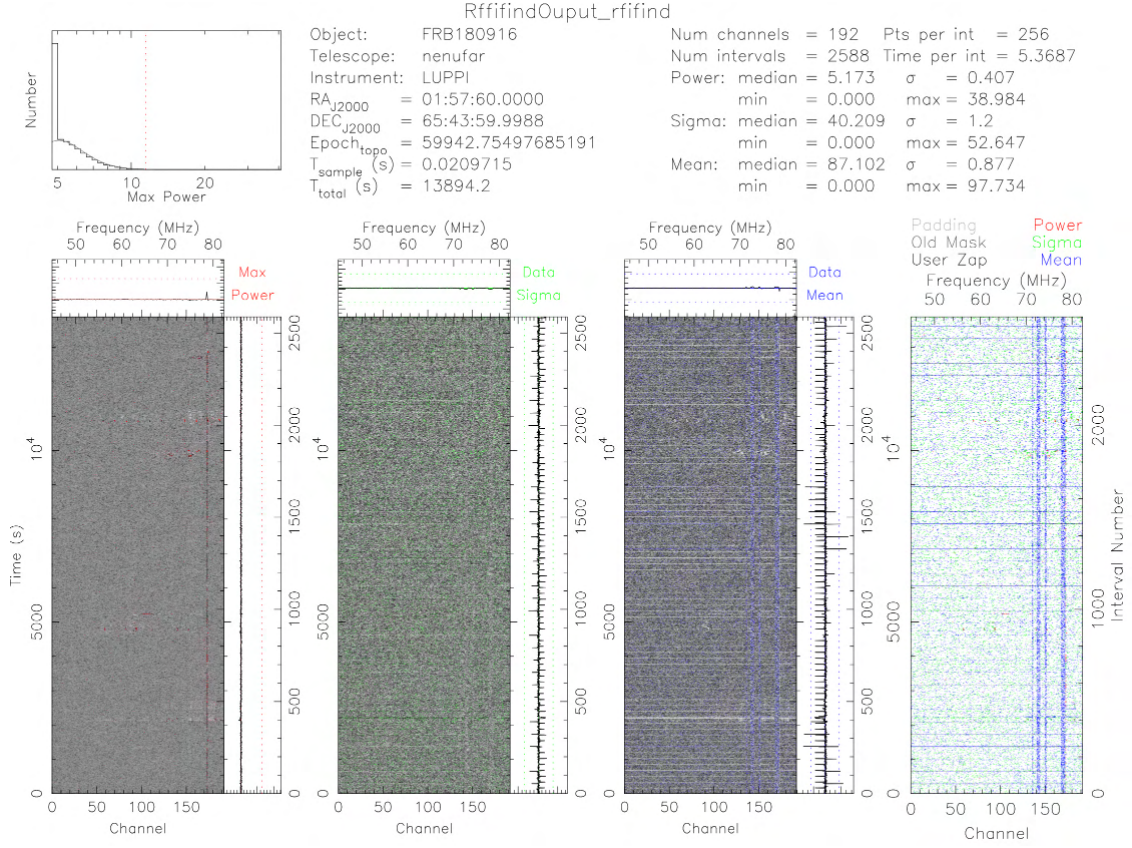
Figure 3.3: Information related to the processing of the observation by RFIFIND to mask the detected RFI. At the top are the data related to the processed observation. The three vertical plots on the bottom left represent the different filters used. The horizontal rectangle on the right represents the resulting mask. Each rectangle represents the dynamic spectrum of the observation with the frequencies in (MHz) and the frequency channel numbers in x and the time in seconds and the time interval numbers in y.
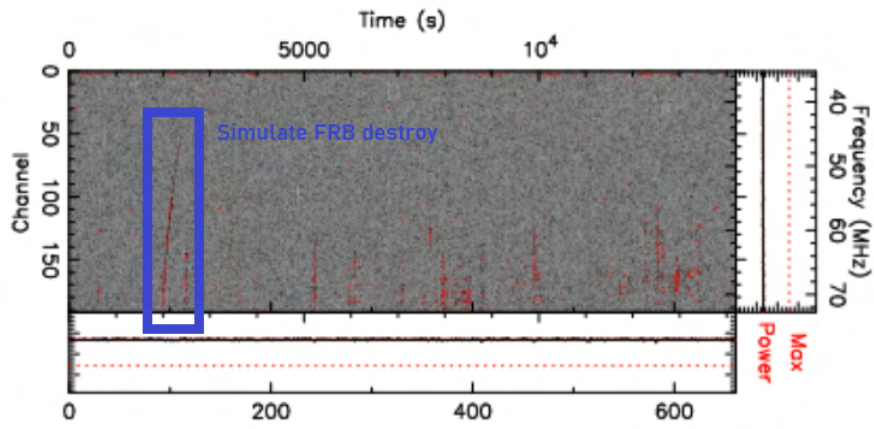
Figure 3.4: Simulated FRB caught by RFIFIND. It's a dynamic spectrum with the time in seconds on the X axis and the frequency in MHz on the Y axis. In the blue square, a simulated FRB is considered as an RFI.

3.1.2   Detection Processing

The burst detection part uses two scripts, one to dedisperse the signal, PREPSUBBAND, and a SINGLE-PULSE-SEARCH algorithm to detect potential bursts and calculate their SNRs (Signal-to-noise ratio).

The idea of the detection part is to take a window of DM around the DM units of the FRB that we want to observe. In our case we take a window of more or less 20 DM units around it. The first script, PREPSUBBAND dedisperses the observation for all the DMs within the window at a given step, in our case 0.01 DM unit. The idea of using a window is to avoid false detections. If an astrophysical object is present at a particular DM, it will also be present at the DM close to it. We will therefore have an signal-to-noise ratio (SNR) peak in a radius close to the target DM. Secondly, the SINGLE-PULSE-SEARCH script performs matched filtering using a boxcar. The closer the dedispersed burst is to the box, the higher the SNR. Figure 3.5 shows the output image of the detection part,it's an NenuFAR FRB observation output. At the top is information about the observation, such as its name, position and samples. Below are 4 plots, the only ones really interesting for detection, apart from the SNR vs DM (top right) and DM vs Time (bottom) plots, the other two are interesting for pulsars. We'll skip the explanations for them.

The SNR vs DM plot (Figure 3.5 , top right plot) shows all the locations in the observation where an SNR greater than 5 was detected, it's the script detection condition, sorted according to the DM tested. The Time vs DM plot (Figure 3.5 , bottom plot) shows the distribution of all detected points by time and DM. So when we observe something, we would have a grouping of points around the DM of the physical object and at the particular time it was detected. (see Fig 3.17) We can therefore use this type of plot to check whether the observation is a potential candidate or not.
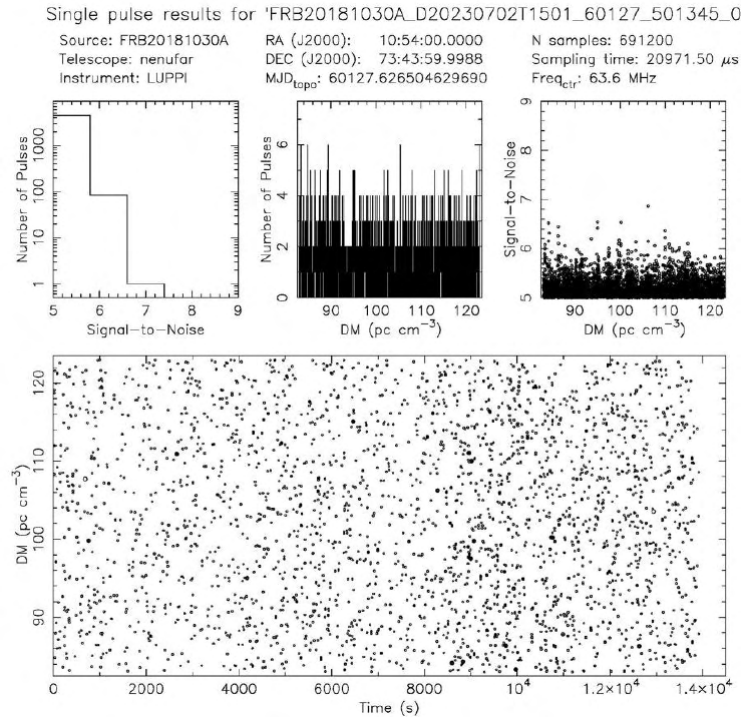

Figure 3.5: The result of the pipeline. The figure shows the output of the pipeline. At the top we can see the information about the observations. Below the information are three square plots. In the top middle is the DM vs pulse count, on the right is the SNR vs DM plot and the one on the left is not really interesting for our study. The bottom plot shows the DM vs Time plot.

3.2   Pipeline Optimization using Pulsar B0329+54

In the previous section we looked at the pipeline we have set up and the various parameters. The size of the observation blocks defines the size of the temporal blocks on which the processing takes place. And the four RFIFIND parameters (SigmaF,SigmaT,BerrT,BerrF) which optimise the RFI suppression. In this section we'll try to understand these parameters and the effect they can have on burst detection. To do this we will first look at pulsar observations. We'll take an observation with many detected pulses and try to optimise the parameters to maximise the output SNR. To do this we will look at the observation of the pulsar B0329+54 and set the size of the observation blocks to 1024 points, i.e. 20 seconds (Figure 3.12a shows the observations used). First, we want to optimise the following four parameters for the RFI cleaning:

- SigmaT: Time Standard deviation

- SigmaF: Frequency Standard deviation

- BerrT : percentage of freq flagged to remove one time subintegration

- BerrF : percentage of time flagged to remove one freq channel

3.2.1   Rfifind Parameter

Pulse Optimization

Pulsars were our first astrophysical object to be studied by the pipeline. In fact, they are good observations to test and optimise the pipeline. After checking that the pipeline is working properly, we look at the variation in the SNR calculation for some pulses of this pulsar observation. The idea is to recover, in addition to the pipeline output plot, the SNR information for some pulses as if they were bursts of FRBs, and then try to see how they behave as a function of the rfifind parameters. Figure 3.6 shows what the recovered pulses look like. The pulses are dedispersed at the pulsar's DM, i.e. 26.7 pc.cm^{-3}.

We then recovered 20 pulses with good characteristics on the pulsar and obtained Figure 3.7. This is a 3D plot of the SNR variation of each of the previously recovered pulses as a function of the SigmaT and SigmaF parameters presented earlier, with berrT and berrF set to 50%. SigmaT and SigmaF varying from 0.5 to 10 with a step of 0.5. These pulses are defined by their detection times on the label of the figure, so each point of the same colour represents the same pulse but with different parameters. The graph appears cloudy, but there are some peculiarities in the variation of the bursts as a function of the parameters. Firstly, the value of the THRESHOLD in time (SigmaT) seems to be crucial for the calculation of the SNR. Below SigmaT < 2 no bursts are detected and above 3 we observe something stable. Figure 3.8 shows the variations in Sigma F, which are not necessarily clear on the 3D plot. This 2D plot, taken with SigmaT fixed at 3, shows us the variations of the SNR of the 20 pulses as a function of SigmaF. We can see that the highest SNRs are obtained for SigmaF close to 0. However, not all pulses are detected for these values.
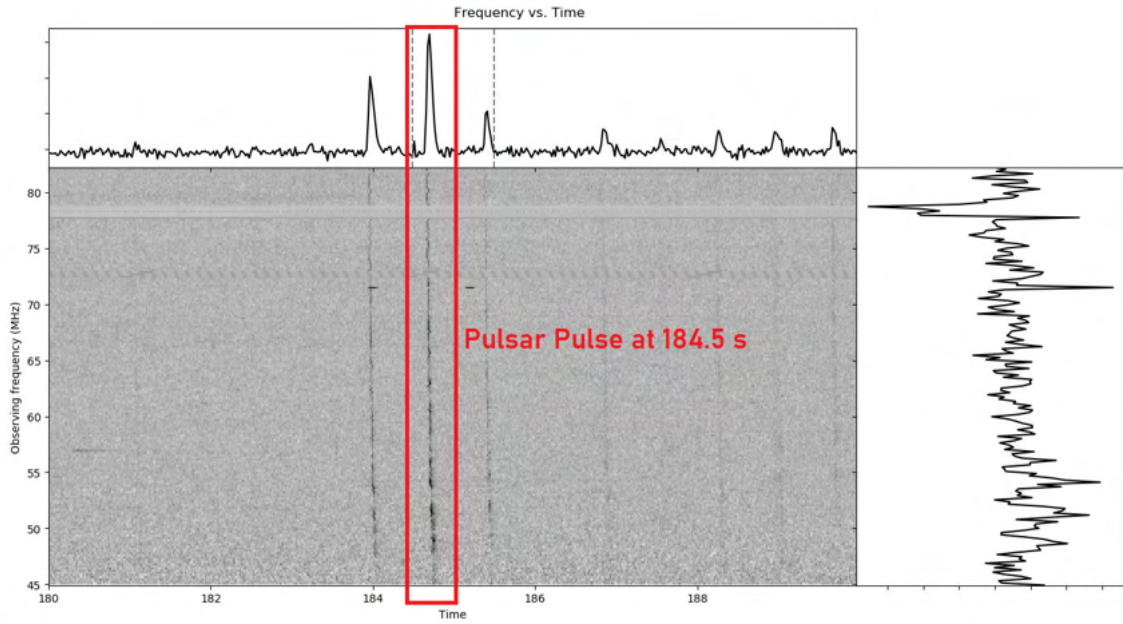
Figure 3.6: Dedispersed dynamic spectrum of a pulsar pulse ((B0329+54, rotation period : 0.714s).This is a dedispersed dynamic spectrum with time in x and frequencies in y. The dynamic spectrum is integrated in time (right plot) and frequency (left plot).The red rectangle window represents one of the pulses considered for this pulse optimisation

We can then go two different ways: reduce the value of the standard deviations to be more selective on the pulses, but allow better SNRs on these few pulses, or look at the observation not through a few pulses but statistically. This is the second method we tried. The aim is to detect as many pulses as possible so that the SigmaT and SigmaF parameters are less destructive. The statistical method is more interesting from an FRB search point of view. In fact, we estimate that we will find at most one single FRB burst in a given observation, if there is one at all. Therefore, choosing an optimisation where we consider the detection of the maximum pulse would make it possible not to miss the possible FRB. In fact, the first method is useful if we know there is a burst and where the pulse is in the observation. But you can miss it if the parameters are not optimised for the pulse. The parameters are over-optimised for only one pulse. The second method, the statistical method, is more permissive and can avoid passing next to a possible burst.
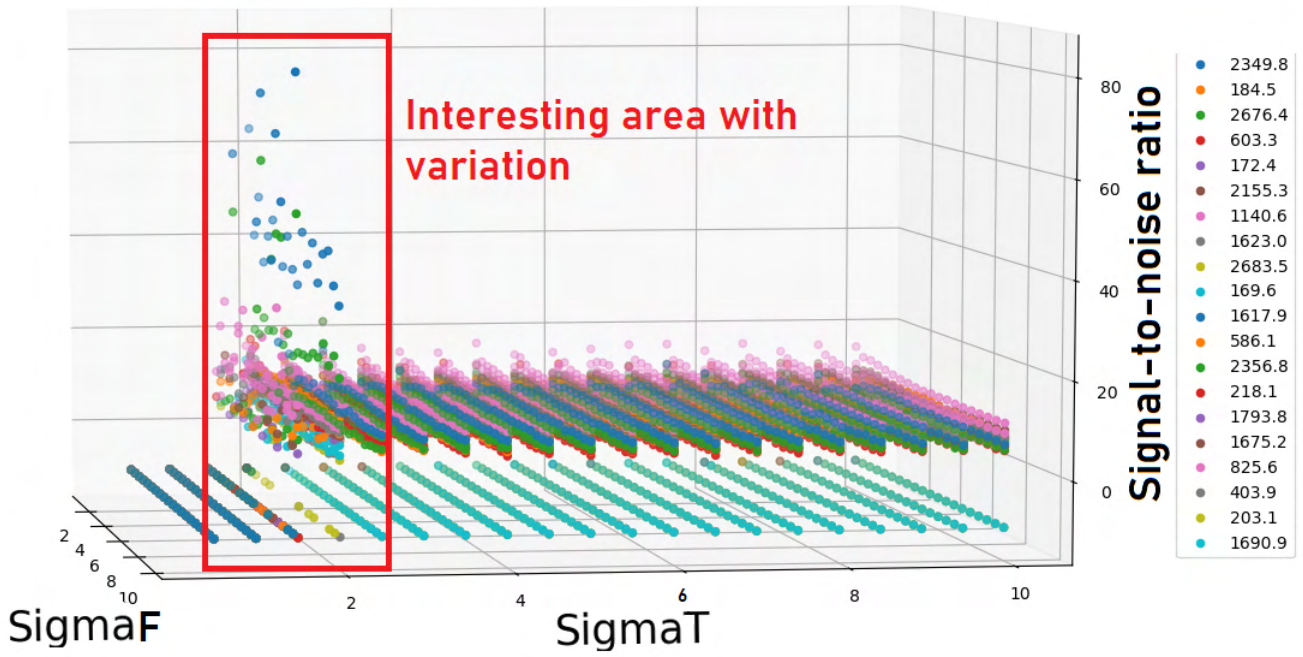
Figure 3.7: 3D image of pulse variation as a function of Rfifind parameters. This is a 3D plot showing the variation of the SigmaT (time threshold) parameter on the X axis, the variation of the SigmaF (frequency threshold) on the Y axis and the signal-to-noise ratio on the Z axis. There are 20 different pulses studied in this plot, represented by 20 different colours defined in the legend on the right. Each pulse is defined by its time position in the observation.
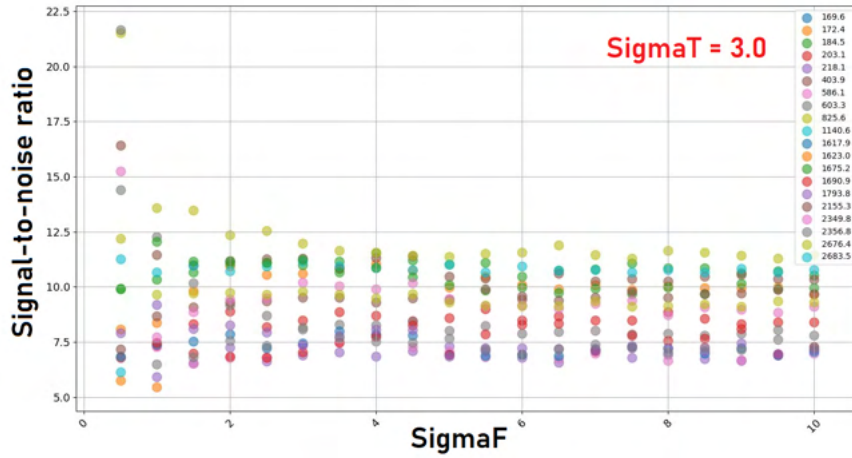
Figure 3.8: 2D section of Figure 3.7 for SigmaT=3.0. On the x-axis are the variations in sigmaF and on the y-axis the signal-to-noise ratio. Each colour represents a pulse defined by its temporal position in the observation (right legend).

Statistic Optimization

The idea is to use the previous pipeline (Fig 3.1) and the SNR vs DM plot and calculate the number of detected points in the DM range that we want to maximise. For a pulsar with a known stable dispersion measurement , good detections are those found within a window of 0.1 pc.cm^{-3} around the theoretical DM of the pulsar. To make a comparison between good and bad detections, we consider all detections found within a window of 20 DM around the theoretical DM in this study, i.e. a window of 40 pc.cm^{-3}.

$$Detection\_rate = All\_hits\_at\_good\_DM/(All\_hits - All\_hits\_at\_good\_DM) * 100 \qquad (3.1)$$

where Detection_rate is the ratio of point detections found on the right DM to all the points detected, All_hits_at_good_DM is the number of potential detections found on the right DM, and All_hits is all potential detections found on all DMs.

The detection ratio defined by the equation 3.1 is a good indicator for finding the maximum number of pulses. It represents the ratio of pulses detected on a good DM to the total number of points processed. As a reminder, a point is detected if its SNR is greater than 5. Thus the detection rate approach is used to optimise the rfifind parameters to detect the most pulses from the pulsar. With four parameters, the simplest approach was to first optimise two parameters by setting the other two and then to do the opposite by setting the first two to their optimum values.
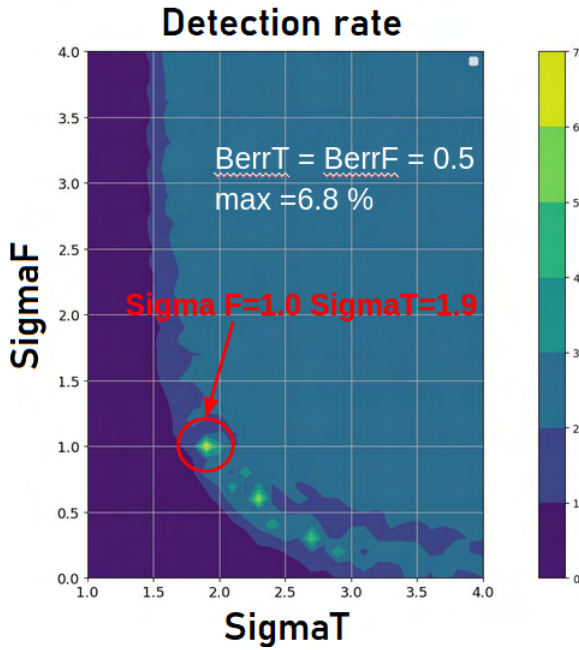

Figure 3.9: Detection rate optimisation using SigmaT and SigmaF. On the x-axis, variations in SigmaT, on the y-axis, variations in SigmaF for a step of 0.1. The colours represent the detection ratio according to the values of the colour bar on the right, yellow for points with a good ratio and blue for poor ratios. For this figure, BerrT and BerrF are set to 0.5. The maximum is given on red circle
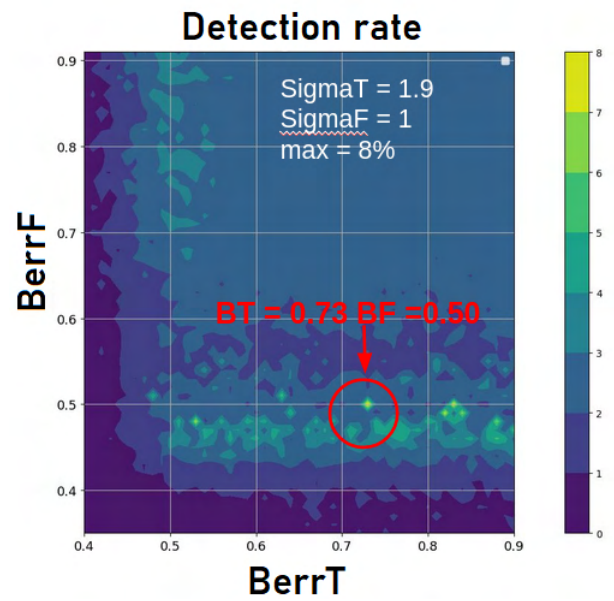
Figure 3.10: Detection rate optimisation using BerrT and BerrF. On the x-axis, variations in BerrT , on the y-axis, variations in BerrF for a step of 0.01. The colours represent the detection ratio according to the values of the colour bar on the right, yellow for points with a good ratio and blue for poor ratios. For this figure, SigmaT and SigmaF are set to the optimum value found in Figure 3.9. The maximum is given on red circle

Figure 3.9 shows the results of optimising SigmaT (ST) and SigmaF (SF). BerrT and BerrF are fixed and the colour scale represents the pulsar detection rate. To produce this plot, we ran the pipeline on the same observation, varying SigmaT and SigmaF. We found a maximum ratio of 6.8, which is 10 times higher than the ratio in the window we looked at. This can be considered a good result. As a reminder, we consider 0.3 of the DMs on a scale of 40, i.e. 0.75 percent of the band. It is interesting to note that for sigmaT and sigmaF we remain in the zone detected by the study of pulsar pulses. (section 3.2.1) Figure 3.10 shows the result of optimising BerrT and BerrF with SigmaT and SigmaF fixed at the value of the maximum

obtained in the previous figure. We can also see a trend around BerrF between 0,45 and 0.5. A maximum ratio of 8% is obtained for the following parameter values SigmaT = 1.9 SigmaF = 1.0 BerrT = 0.73 BerrF = 0.50.

The interesting thing about this study is that the maximum values can be defined as singularities. They are separated from places where nothing is detected. So for close parameter values the ratio varies a lot. On the other hand, we can show that for different parameter sets the results are quite different and that for most of them the ratio is not high. This raises the question of whether we are overparameterising the observation.

Figure 3.11: Detection rate optimisation using SigmaT and SigmaF. On the x-axis, variations in SigmaT, on the y-axis, variations in SigmaF for a step of 0.01. The colours represent the detection ratio according to the values of the colour bar on the right, yellow for points with a good ratio and blue for poor ratios. For this fig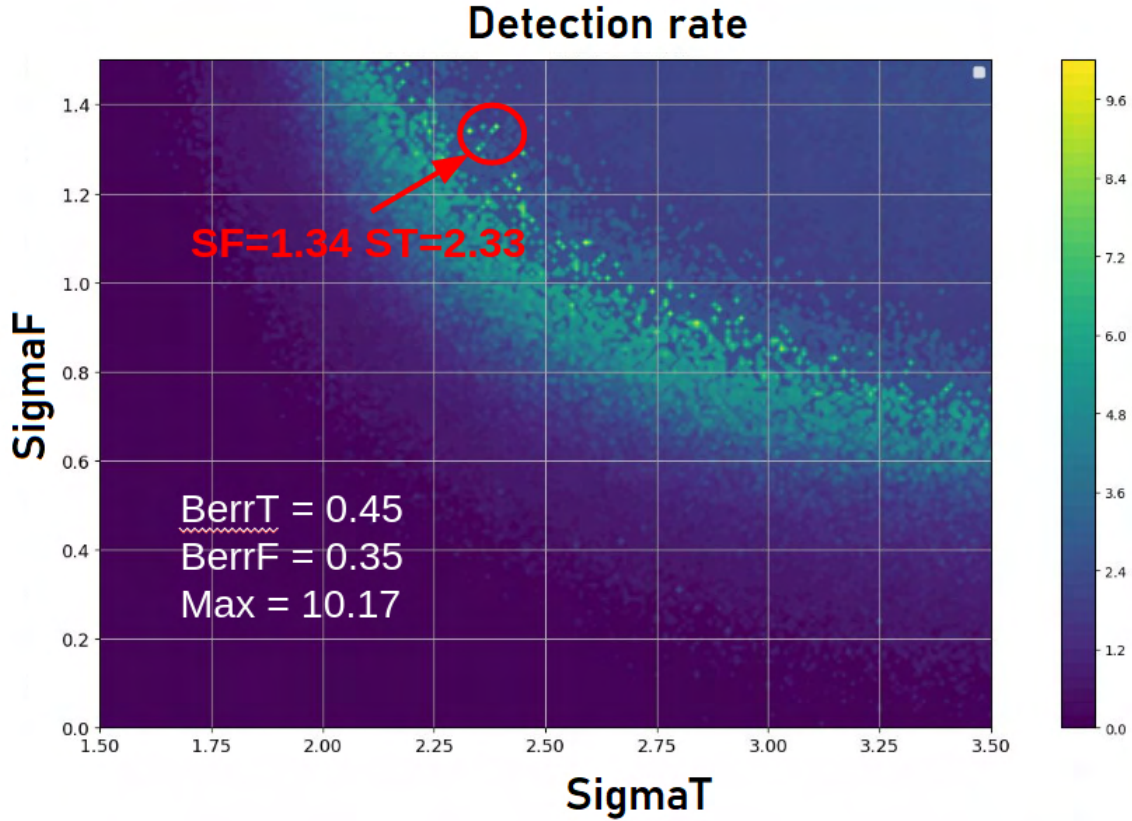ure, BerrT and BerrF are set to the optimum value obtained in the same way as for the figure 3.10 (BerrT = 0.45 and BerrF = 0.35). The maximum is indicated by the red circle.

To compare the results, Fig. 3.11 shows the same study as above on the same observation, but in the opposite direction. We first optimised BerrT and BerrF by fixing SigmaT and SigmaF, and then optimised SigmaT and SigmaF. The result is a ratio of 10.17, which is a clear improvement. However, it should be noted that the optimum parameters in this plot are different from those in the previous study. The optimum parameters are SigmaT = 2.33 SigmaF = 1.34 BerrT = 0.45 BerrF = 0.35. There is some relationship between these two maxima. The first study had smaller SigmaT and SigmaF values, implying greater signal filtering, but larger BerrT and BerrF values to avoid suppressing too much of the signal. The second study achieves the opposite, where SigmaT and SigmaF filter the signal less, but BerrT and BerrF are smaller, implying greater channel suppression.

On the other hand, in this plot the high ratios follow a certain law defined by SigmaT and SigmaF. The same curve was present in figure 3.9. There is therefore a correspondence between

these two studies.
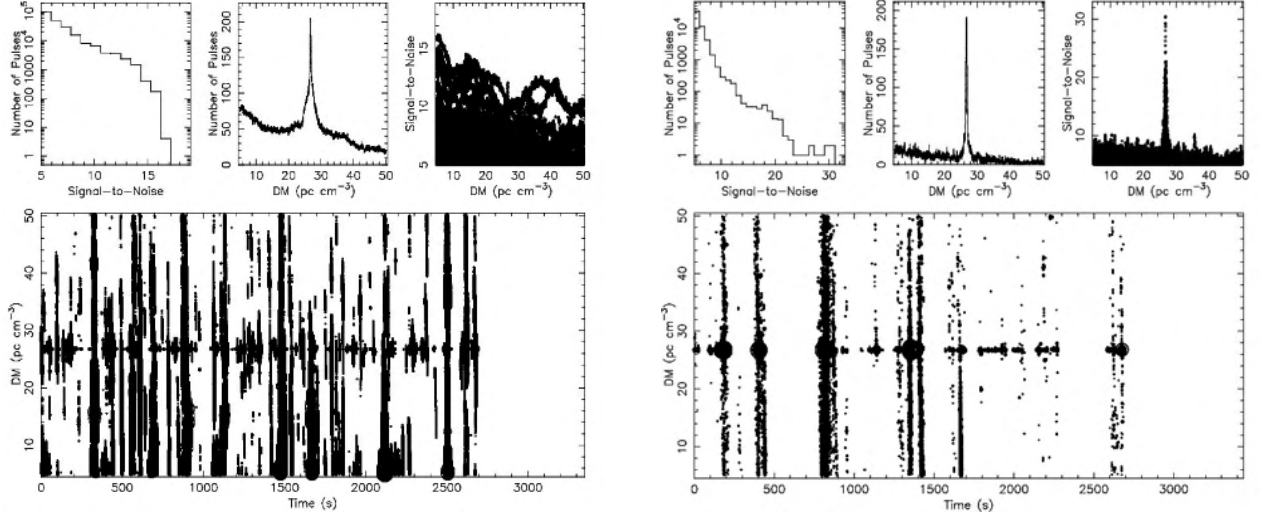
(a) DM vs Time plot of the pulsar observation process through the pipeline without parameter optimisation of this pipeline.

(b) DM vs Time plot of the pulsar observation process through the pipeline with optimal parameters.

Figure 3.12: Comparison of pipeline results with non-optimised parameters on the left and optimised parameters on the right. The two interesting plot are the SNR vs DM plot at the top right and the DM vs Time plot at the bottom of each figure. Each detected point on either the SNR vs DM or DM vs Time plot represents a possible detection. They are selected if the signal at the coordinate of the point (DM,Time) has an SNR greater than a certain threshold, in this case 5.

To conclude on the optimisation of this pulsar observation, it is interesting to compare the SNR vs Time plots obtained for the non-optimised observation and the optimised optimisation with the correct rfifind parameters. The block size for the observation was set to 1024 points, i.e. 21.4 seconds for this section. Figure 3.12 shows this comparison between the unoptimised and optimised observations. Looking at figure 3.12a, i.e. the unoptimised observation (SigmaT = 3, SigmaF=3 BerrT=0.5 BerrF=0.5), we see significant saturation or RFI for most of the DM bands, as can be seen in the SNR vs DM plot (top right) and the DM vs Time plot (bottom). The pulsar can still be distinguished by the appearance of a line at DM 26.7 on the DM vs Time plot. However, the SNR found on the SNR vs DM plot (top right) provides no information about the detection of the pulsar. Worse, the highest SNRs are obtained on RFI. In contrast, the optimised version (ST = 1.34, SF=2.33, BerrT = 0.45, BerrF = 0.35) shown in Figure 3.12b gives much better results. The SNR vs. DM plot (top right) shows a large spike at the desired DM, i.e. 26.7. It can be seen that the SNR around this DM is greatly reduced, allowing only the pulses of interest to be detected. Finally, the DM vs time plot is much less saturated than that of the first observation, which also allows better detection.

We then carried out the same study on several other observations and observed variations in the most optimal parameters. The trends don't change completely, but the values are still different. SigmaT and SigmaF around [] Nevertheless, the study is interesting because it shows the possible optimisation that can be achieved by looking only at an observation that we considered interesting.

3.2.2   Block Optimisation

The final parameter to consider when optimising this pipeline is the observation block size. Initially we chose the maximum, i.e. 21.4 seconds, because the FRBs are really dispersed.
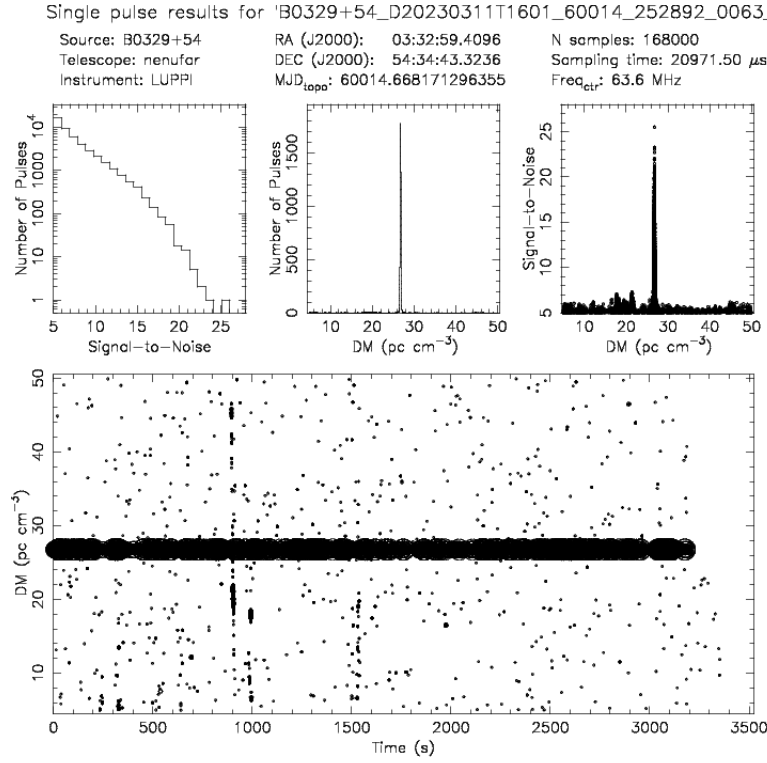
Figure 3.13: Pipeline result for a good block size on the pulsar observation. Figure obtained with SigmaT = 3.5, SigmaF = 3.5 BerrT = 0.5 BerrF = 0.5 and a Block Size of 32 points (0.67s).

So it's important to use long blocks to avoid destroying too much information. On the other hand, the big problem with using blocks with many points is that they also let in more noise. To demonstrate this, we continued the previous study using the same pulsar observation. To quickly describe the allowed block sizes, there are 6 different block sizes that can be used, 32 points, 64 points, 128 points, 256 points, 512 points and 1024 points, i.e. 0.67s, 1.3s, 2.7s, 5.3s, 10.7s and 21.4s respectively.

For this pulsar, Figure 3.13 shows the result for a more appropriate block size. Here the block size is 32 points. This figure is made with non-optimal rfifind parameters, but we can see a clear improvement in the observation. Some RFI is still present (bottom plot), but a pulsar is extremely visible at 26.7 pc.cm^{-3} on all plots in the figure.

A more detailed study will be carried out in the next section to define the ideal block sizes for FRBs, as the pulsar study is not very informative about the choice of blocks for FRBs. In fact, the pulsars we have studied are not very dispersed. In addition, this pulsar has very bright pulses (close to Earth) and this leads strongly favours block sizes that are very destructive to RFI (few points). The pulses are so bright that they are inevitably detected. This is not the case for expected FRBs.

Finally, the pulsar optimisation. Figure 3.14 shows, on the left, the initial observation and the observation finally processed with the optimal choice of blocks and the optimal rfifind parameter. The difference is really striking and encouraging for the study of FRBs. On the other hand, the study of pulsars breaks down in certain physical aspects (as scattering) and it becomes necessary to carry out a simulation of an FRB to continue this pipeline optimisation.
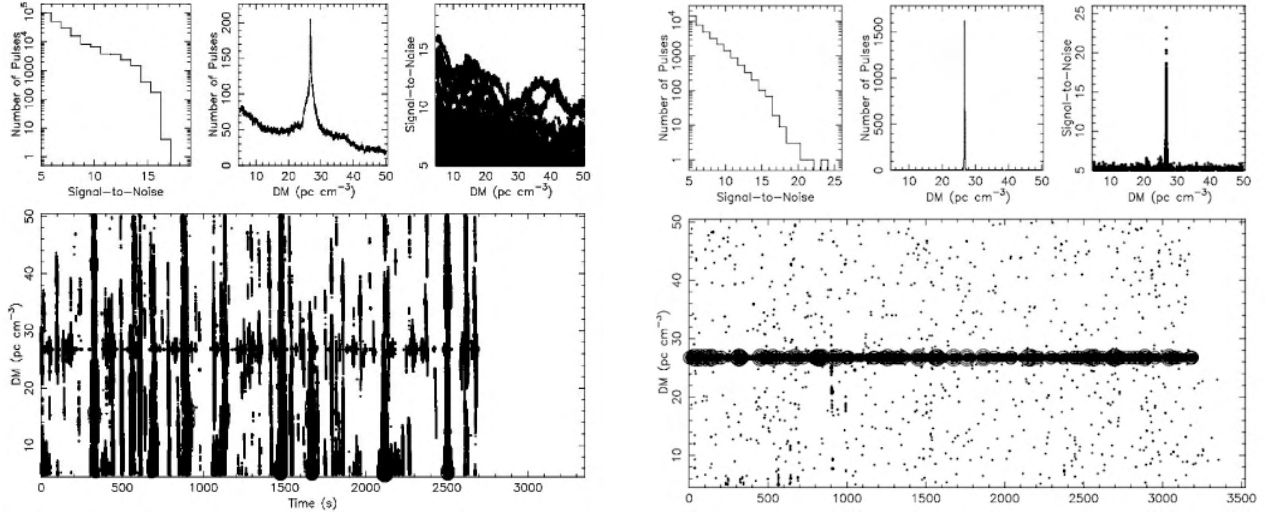
(a) Pipeline result for the pulsar observation without any optimisation

(b) Pipeline result for a good block size and a good settings on the pulsar observation

Figure 3.14: Comparison between an observation treated in a non-optimised way, on the left, and an observation treated with good parameters, on the right.

3.3 Simulation

In order to carry out this simulation, we had to study different aspects of the FRB. The simplest idea to reproduce the dynamic spectrum of an FRB was to reconstruct the signal frequency channel by frequency channel. The solution adopted was to use an identical Gaussian for each frequency channel. The first thing to implement was the dispersion, Equation 1.2, where the DM is known due to the choice of repetitive FRBs, namely 348.9 pc.cm^{-3} for FRB20180916B and 218.9 pc.cm^{-3} for FRB20220912A. Figure 1.3 is a simulation of the dispersion obtained. The time-frequency shifts are clearly visible. Next, we had to implement the scattering. The idea was to convolve each frequency channel previously constructed by an exponential according to the equation 3.2.

$$\text{SimulatedSignal}_i = \text{ChannelFreq}_i * \left(\exp\left(-t/\tau_i\right) U(t)/\tau_i\right) \tag{3.2}$$

where ChannelFreq$_i$ represents the frequency channel number i ,t is the time in seconde $U(t) = 1$ si $t >= 0$ et 0 sinon, τ_i is defined in the equation 3.3 and SimulatedSignal$_i$ represents the scattered simulated signal for frequency band number i.

$$\tau = \text{ScatteringTimeAt600MHz} * \left(\text{CentralFrequency}/600\right)^4 \tag{3.3}$$

where τ represents the characteristic scattering time for this frequency, ScatteringTimeAt600MHz represents the characteristic scattering time of this FRB found at 600MHz and CentralFrequency represents the center frequency of one channel.

Figure 3.15 is a representation of the scattering phenomena defined by Eequation (3.2). As before, the dynamic spectrum of the simulated burst is shown with frequency integration on top and time integration on the right. Figure 3.15a shows only the scattering for FRB20180916B, an FRB with a scattering time of 1.05 ms at 600 MHz. The phenomenon studied in section 1.14 is relatively important for distant astrophysical objects. Initially the burst is Gaussian with a mean of 100 s and a standard deviation of 0.5 s. The figure shows that the burst has a width of about 100 s at a frequency of 40 MHz and three seconds at 80 MHz. The broadening of the pulse is therefore not trivial, unlike for most pulsars. Figure 3.15b shows the scattering phenomenon, but with energy conservation. It is first assumed that the burst is emitted in
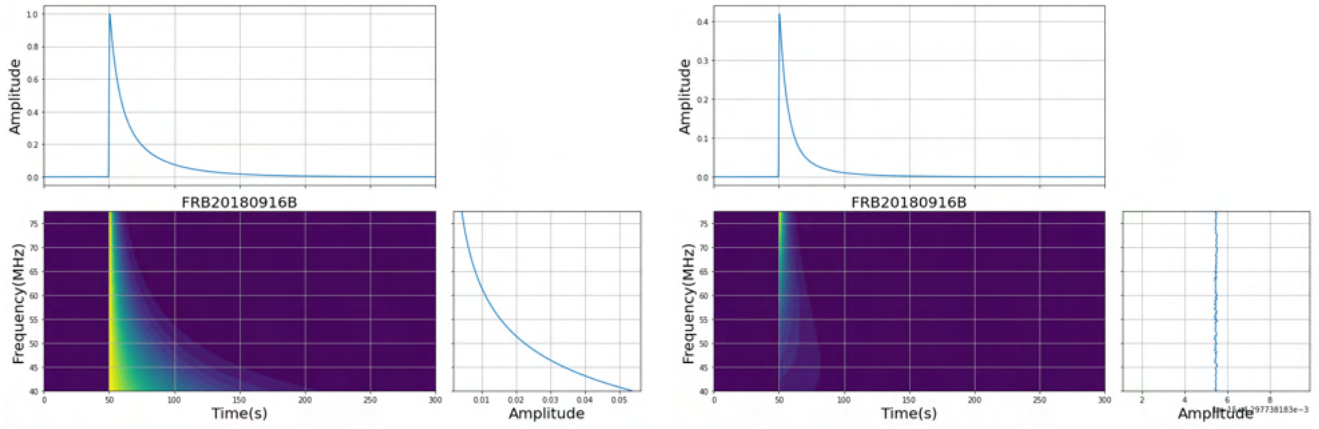
(a) Simulation of the scattering phenomenon without conservation of energy

(b) Simulation of the scattering phenomenon with conservation of energy

Figure 3.15: Simulation of the scattering phenomena at FRB20180916B. On the left is the simulation without energy conservation and on the right is the simulation with energy conservation. Each plot consists of a dynamic spectrum in the middle, a frequency integration plot at the top and the time integration plot on the right. The x-axis is the time in seconds and the y-axis is the frequency in MHz. The colour variations represent the different intensities in the simulation. Light for high intensities and dark for low intensities.

the same way at all frequencies. It is therefore necessary to assume that scattering does not add energy as frequencies decrease. Figure 3.15b is obtained by normalising each frequency channel. It can be seen that low frequencies become very weak due to their large scattering. To complete and correct this simulation, the scattering and dispersion must be combined. We also add a polynomial function to the amplitudes of the initial Gaussian to simulate the bandwidth of the radio telescope. The radio telescope is more sensitive around 60 MHz. Frequencies close to 80 and 30 MHz have reduced sensitivity or even zero at the extremities. Figure 3.16 shows the simulation of FRB20180916B on the left and FRB20220912A on the right.

To define a simulation, we need to consider four different parameters. Burst width, burst amplitude, scattering at 600 MHz and DM. As the last two parameters are linked to the choice of the FRB source, they cannot be changed. However, it will be interesting to choose a good amplitude and width to simulate our FRB. If we look at the detections of other telescopes that have found these FRBs, it turns out that the width of the initial burst is on the order of tens of milliseconds. So we will use this order of magnitude in our simulations.

The choice of the FRB amplitude is complicated by the fact that the FRB is subject to phenomena that change its amplitude. We have chosen to define the FRB amplitude as the maximum of the simulated signal. If we consider a simulation with an amplitude of five, this means that the maximum energy of the signal at a time-frequency point is five (Not unit telescope measurements are not calibrated). It is important to consider a standard for this. We cannot define a desired SNR at this stage because the FRB has not yet been inserted into the observation. Furthermore, the idea is to insert it before processing the pipeline to produce a simulation that is as close to reality as possible. We can then make correlations between SNR and burst amplitude once the simulation has been run through the pipeline.

The final objective of this simulation was to insert the simulated burst into an observation and then run it through the pipeline. Firstly, to check that our pipeline works, as so far it has only been tested on low DM pulsars. Secondly, to check that the simulation produces a result that matches what we hope to observe.

Figure 3.17 is obtained after running an observation with a simulated burst through the

(a) FRB20180916B simulated   (b) FRB20220819A simulated
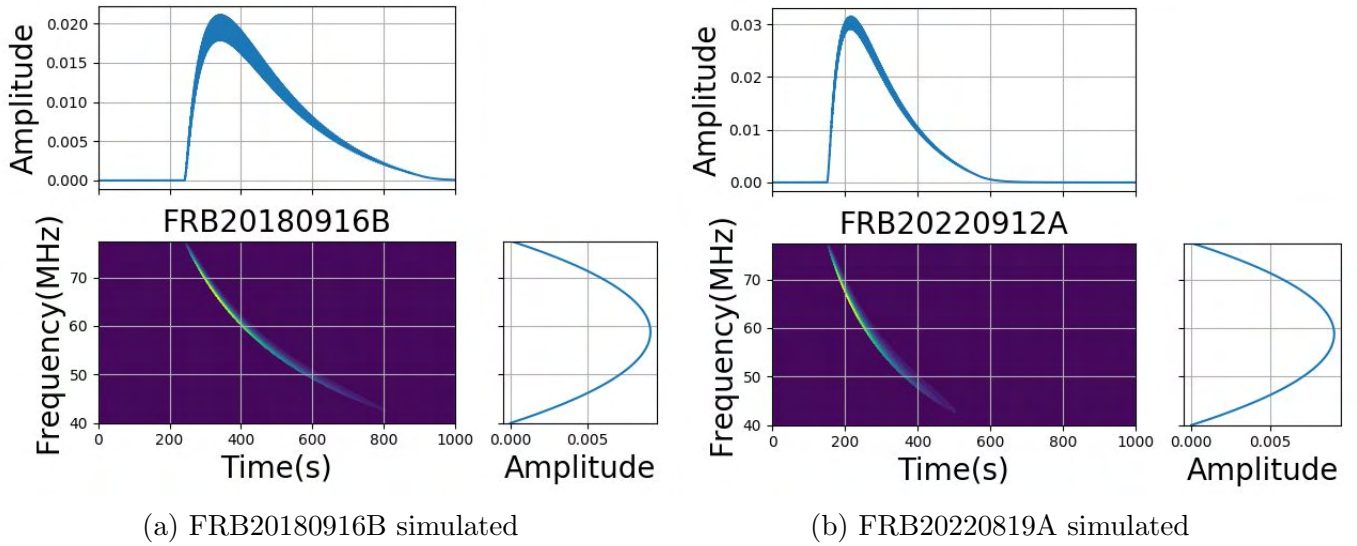
Figure 3.16: Simulation of FRB20180916B and FRB20220912A. On the left, the simulation FRB20180916B and on the right FRB20220912A. Each plot is composed of a dynamic spectrom in the centre, a frequency integration plot at the top and the time integration plot on the right. The x-axis is the time in seconds and the y-axis is the frequency in MHz. The colour variations represent the different intensities in the simulation. Light for high intensities and dark for low intensities

pipeline. It simulates FRB20220912A with a DM of 218.9 pc.cm^{-3} and a scattering time of 1.05ms at 600MHz. We used a burst amplitude of 2 and a pulse width of 20ms. Finally, the parameters used in the pipeline are not very destructive. SigmaT = 3, SigmaF =3 BerrT = 0.5 BerrF=0.5 and the block size is 128 points.

Our simulated FRB is clearly visble in Fig 3.17. It was inserted on the 2000th second of the observation and is well centred on DM 218.9 pc.cm^{-3}. The SNR vs DM plot shows a peak at the desired DM and an SNR of 15. On the DM vs Time plot, a large dot appears at the desired time and at the desired DM. We can therefore validate not only our simulation but also our FRB detection pipeline.

Figure 3.18 is a dynamic spectrum for a DM of 219 pc.cm^{-3} which shows the simulated pulse present in the observation. The time integration at the top of the figure shows a well-dispersed and scattered burst. To explain the result, the burst is not visible at low frequencies because the scattering phenomenon has reduced the burst's amplitude too much. What's more, the burst is scattered over 4 seconds. This is the correct order of magnitude of the characteristic scattering time for this FRB at these frequencies. As a result, it appears complicated to detect an FRB at frequencies below 50 MHz. The burst is so weakened over time that it is becames invisble. One solution to detecting FRBs at frequencies below 50 MHz would be to look for FRB sources with much less scattering phenomena (such as pulsars).

The simulation works. We need to understand the effect of the amplitude and width of the simulated burst. To do this, we ran several simulations with different widths and amplitudes. We obtained the SNR of each after pipeline processing. The rfifind parameters used in this study are SigmaT=3.0 SigmaF=3.0 BerrT=0.5 and BerrF=0.5. These were chosen in response to the study carried out in section (3.2.2). These parameters allow the RFI to be handled correctly without suppressing the burst. The section showed the importance of choosing the right block size when processing the observation. We have therefore also studied the effect of the different blocks on the SNRs obtained for each simulation. Figure 3.19a shows the SNR obtained from the simulation as a function of burst amplitude. Amplitudes between 0.1 and 10 were used. Each coloured dot represents the SNR obtained for a particular processing block
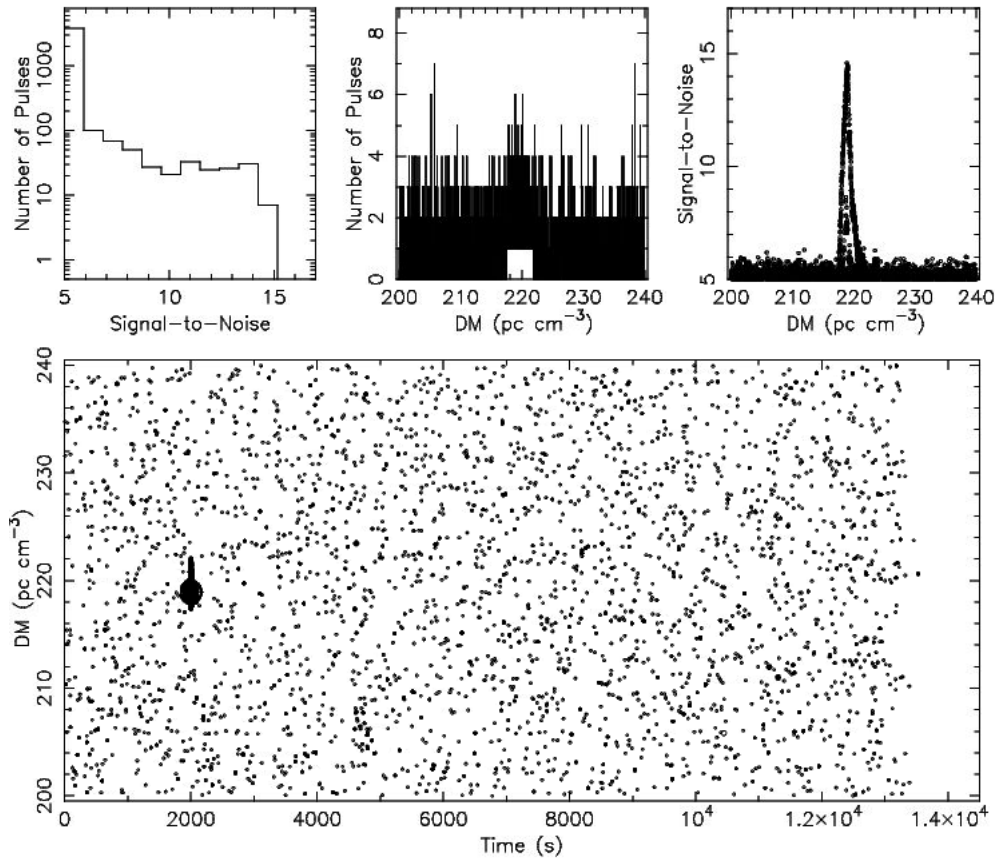
Figure 3.17: Pipeline result for an observation with an simulate FRB inside

size. This results in two different regimes. The first is for small amplitudes, also known as weak bursts, where the burst is at the limit of detection. In this case, large blocks are used to detect the burst. The 10.7 second block size is most appropriate here. On the other hand, in the second regime, for strong bursts with huge amplitudes. The SNR is of course better, but smaller blocks are preferred.

To explain this result, a highly dispersed and scattered FRB is less affected by the flattening that occurs as the block size increases. Weak bursts are therefore more easily detected by large blocks. On the other hand, if the burst is bright, it will greatly modify the statistics of the large blocks and therefore be seen as a possible RFI, explaining the loss of SNR for large blocks and bright burst. It will therefore be interesting to use small blocks to search for bright bursts and large blocks to search for weak bursts. On the other hand, care must be taken not to choose blocks that are too small, as shown by the choice of 0.67 second blocks, where the SNRs obtained are never very interesting. The same applies to blocks that are too large, such as the 21.7-second block, which unfortunately does not handle RFI well enough and therefore gives biased results.
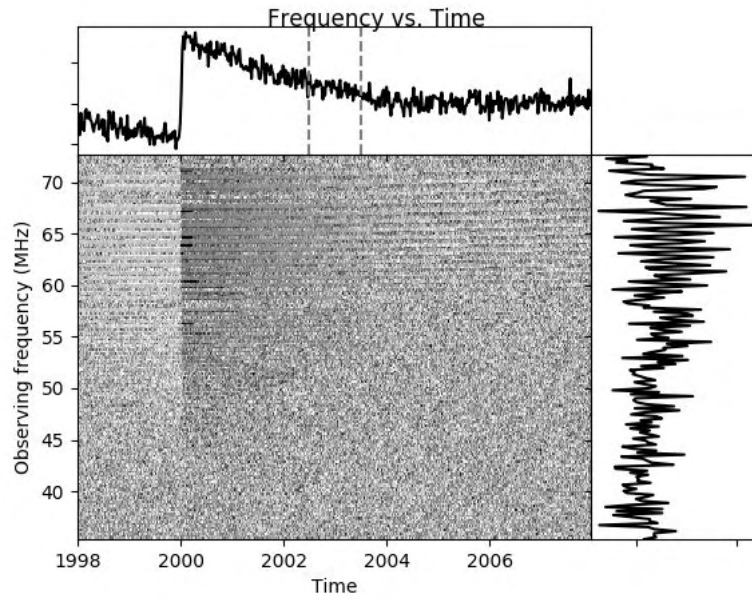
Figure 3.18: Waterfall of a simulated FRB20220912A burst. It's a dedisperse dynamic spectrum at a DM of 218.9 pc.cm^{-3}. On the x-axis, times in seconds and on the y-axis, frequencies in MHz. At the top is the frequency integration and on the right the time integration.

Figure 3.19b shows the SNR obtained from the simulation as a function of the burst width. For this plot, we take a burst amplitude equal to one. It shows that the pulse width has no real effect on the SNR obtained. In fact, the variation is only affected by the choice of blocks (legend in Figure 3.19a), represented by the different colours, and not by the burst width. to conclude this section on the study and optimisation of the pipeline We created a pipeline to process FRBs, then studied its various parameters to optimise the pipeline for FRBs. We then simulated FRBs to further find the right parameters. In the end, we found good rfifind parameters to correctly detect FRBs. Some information about the size of the blocks to choose, depending on the FRB profile we are trying to observe. For example, we know that FRB20180916B has a bright burst profile, while FRB20220912A has a faint burst profile. Use strong rfifind parameters when using small block sizes. (For example, SigmaT=3, SigmaF=3, BerrT=0.5, BerrF=0.5. with a lareg blocks size(256,512,1024 point)) On the other hand, use more permissive rifind parameters on RFIs for large block sizes to avoid FRBs being considered as RFIs. (SigmaT=5, SigmaF=5. BerrT=0.5, BerrF=0.5. small block size (64,128 point)) Large block sizes (256,512,1024 point) should be used to detect weak bursts. On the other hand, for really noisy observations or powerful bursts, small block (64,128 point) sizes will be most effective. Further optimisation would be possible to define the most suitable parameters for each block size.(More information on the appendix 5.3)
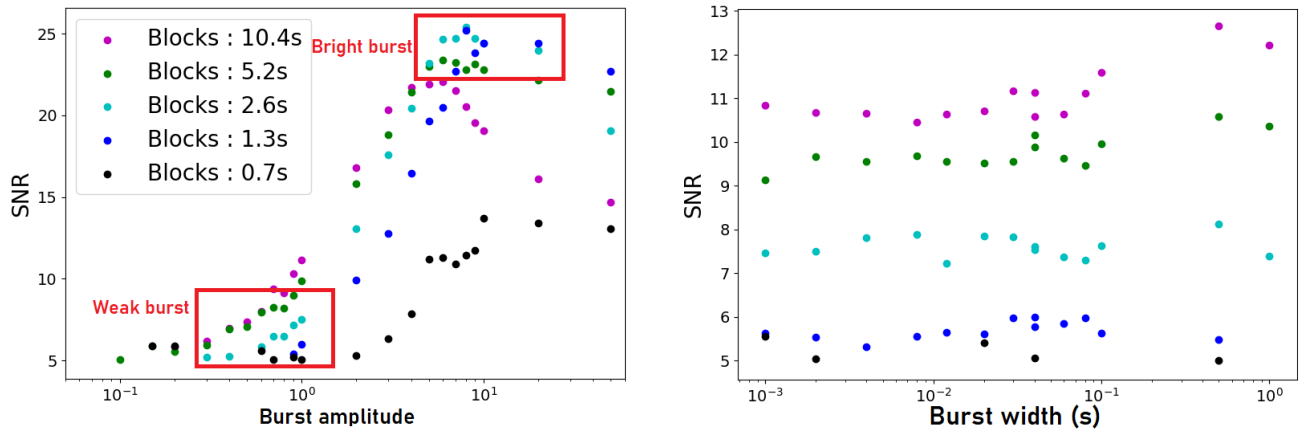
(a) Graphs of the impact of the amplitude of the simulated burst on the SNR found by the pipeline. The width of the simulated burst is set to 10ms.The logarithmic x-axis defines the amplitude of the simulated burst and the y-axis the SNR found at the output of the pipeline.

(b) Graphs of the impact of the simulated burst width on the SNR found by the pipeline. The amplitude of the simulated burst is fixed at 1.The logarithmic x-axis defines the width of the simulated burst en seconde and the y-axis the SNR found at the output of the pipeline.

Figure 3.19: Graphs of the impact of simulated burst characteristics on the SNR found by the pipeline. It's an FRB20220912A simulation. On both graphs, each point represents a simulation processed by the pipeline. The colour of each point is determined by the size of the blocks used during processing. The legend for these colours can be found on the graphs 3.19a

.

Chapter 4

Discussion

In parallel with the pipeline optimisation, all observations were processed to try to find FRBs in the NenuFAR observations.

4.1 Observation processed

Throughout the internship, once the pipeline was up and running, the observations were treated in different ways depending on what was discovered to optimise the pipeline. No FRBs have yet been detected in the observations, but not all the results have been examined.

trial #	Total # files	Which FRBs	Rfifind parameters and Blocks Size	Other comments
1	146	20180916B	-blocks 10.7s -freqsig 3 -timesig 2 -chanfrac .5 -intfrac .5 Ds 8s	Ttc : 1.5 days Result : Nothing found Comment : Too noisy -> Not optimal Ds
2	240	ALL *	-blocks 0.67s -freqsig 3 -timesig 3 -chanfrac .5 -intfrac .5 Ds 1s	Ttc : 2 weeks Result : Nothing found
3	240	ALL *	-blocks 0.67s -freqsig 2.5 -timesig 2.5 -chanfrac .5 -intfrac .5 Ds 1s	Comment: Targeted for Bright FRBs
4	256*4	ALL *	-blocks [0.67s,1.4s,2.8s,5.4s] -freqsig 3 -timesig 3 -chanfrac .5 -intfrac .5 Ds 1s	Ttc : 2 weeks but 4 processing per observation Comment : 2 ways to calculate snr, Not see Yet, need ML
5	256	ALL*	-blocks [2.8s,5.4s] -freqsig 3 -timesig 3 -chanfrac .5 -intfrac .5 Ds 1s -blocks [0.67s,1.4s] -freqsig 3 -timesig 5 -chanfrac .5 -intfrac .5 Ds 1s	Ttc : In Progress Comment : ML and subband Search (around 20MHz)

Figure 4.1: All treatment campaigns completed on NenuFAR observations.This table is divided into five columns. The first defines the number of the treatment campaign performed, the second defines the number of observations treated during this campaign. The third defines the FRBs processed, the next the pipeline parameters used for the processing and the last the comments. ALL * = FRB151125; FRB20180814; FRB20180916B; FRB20180814A; FRB20180908B; FRB20181017A; FRB20181030A; FRB20190303A; FRB20200120E; FRB20220912A

Figure 4.1 is a table showing all the processinf runs applied to the observations. They are listed in chronological order from top to bottom. It contains information such as the names of the FRB sources, the number of observations processed, the parameters used, and the results. Our processing has evolved in line with developments in pipeline optimisation. First we did a primary campaign to check the pipeline and see if there was anything obvious in the observations. Then we realised that all the observations were full of RFI and we ran much

more specific trials. Trail 2 and 3 were run with a block size of 0.67s to detect only bright bursts. Unfortunately nothing was found except one candidate which turned out to be a faulty electronic amplifier (see on 5.4). Finally, the last two trials were run after the simulation had been set up. We are therefore using the information from this simulation, such as optimising the block and rfifind parameters, to focus more specifically on detecting weak bursts. The results of the last two trials have not yet been analysed. With over 1,000 plots to look at, we decided to use a machine learning algorithm to process the results automatically, but the algorithm is not yet fully functional.

Visually, there are a lot of possible candidates for small bursts. We could look at each plot and then look at the observation at the appropriate time to see if there is an FRB. But that seems tedious. The results of the various attempts take two different forms. The DM vs Time plot presented in the previous sections, but also a text file necessary for using the machine learning algorithm. All this is neatly arranged and classified in a directory according to the names of the FRB sources, the dates of the observations and the trial number. This makes it possible to monitor the processing and the results obtained for each NenuFAR observation.

4.2 Weekly Report

The NenuFAR radio telescope performs new observations of FRBs every week. In order to monitor the observations on a regular basis, we have set up a NenuFAR Weekly Report. The idea is to compare the already processed observations with the new ones. Fig. 4.2 shows an example of this report. Firstly, we have a report containing information about the observations made during the week. Secondly, the report processes the observations through the pipeline, adjusting the parameters according to the astrophysical source we are looking at. It then emails back the pdf of the report produced i.e, a summary of the observations made during the week and the results of the observations processed by the pipeline. This makes it easy to see if the observations are interesting or not. For example, you can see if the observation is noisy, if it has patterns that could be reminiscent of FRBs, or if there is a problem with the observation.
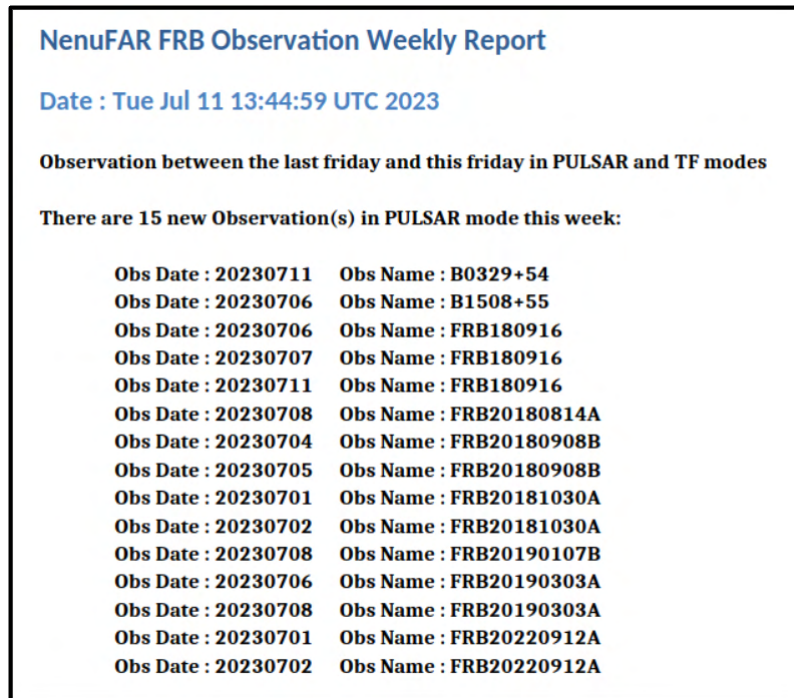

Figure 4.2: NenuFAR weekly Report

4.3   Next Steps

There are two main directions for continuing the work that has been done. The first is to adapt the machine learning algorithm to look at results that have not yet been looked at. For a quick description, it can be divided into two parts. SPEGID is a nearest neighbours algorithm and FETCH is an algorithm that takes the result of SPEGID, i.e. the coordinates of a possible burst in an observation, and applies a convolutional neural network directly to the dynamic spectrum of the observation to the coordinates of the candidate detected by SPEGID. The idea is that SPEGID finds potential candidates by clustering points around the desired DM, and that FETCH then detects whether or not the burst is an FRB directly in the observation. Currently SPEGID works, it detects and finds the exact coordinates of simulated bursts, but FETCH does not work. This needs to be fixed. (see more detail in appendix 5.2) Also, the observations processed by the pipeline all have an output that can be read by SPEGID. The remaining part is to get FETCH to work properly[1].

Finally, the second part would be to look at the observations not over the whole telescope band, i.e. 37.5 MHz, but in smaller 10 MHz bands. Another team (LOFAR Team) of researchers looking for FRBs at frequencies around 140 MHz (LOFAR) is using exactly this method to increase their chances of finding FRBs and their detections confirm this[10]. A new survey with this functionality would have to be implemented to have any hope of finding anything. However, the relevance of this study in our case remains to be define by the fact that an FRB only appears detectable above 50MHz (Fig 3.15) because of its scattering. This leaves only 2 to 3 sections of 10MHz. We have shown that scattering at frequencies of 50 MHz makes the pulse virtually undetectable. One solution might be to concentrate only on frequencies close to 70MHz, where the burst remains detectable.

4.4   Conclusion

To conclude this M2 internship, the main objective was to look for FRBs in the NenuFAR observations. To see if it was possible to detect fast radio bursts on a new frequency band (30 MHz to 80 MHz). The internship was motivated by the fact that the closest and lowest frequency FRB ever detected was found by the LOFAR Radio Telescope teams at a frequency of 110 MHz[19]. Just above the NenuFAR band. To do this, I created a pipeline to process the observations and optimised it by running a simulationthat i did[9]. I was then able to apply several processing methods to each observation with a view to finding FRBs. Unfortunately, I have not yet detected FRBs in the observations made by NenuFAR, but I have implemented tools such as the Nenufar Weekly Report to provide weekly reports and facilitate the automatic processing of observations. I was also able to classify the observations and more generally the source FRBs to determine their relevance. This internship is a first approach to FRB detection on NenuFAR. There are still a lot of unseen results and I hope to believe that there is possibly a FRB inside.

Chapter 5

appendix
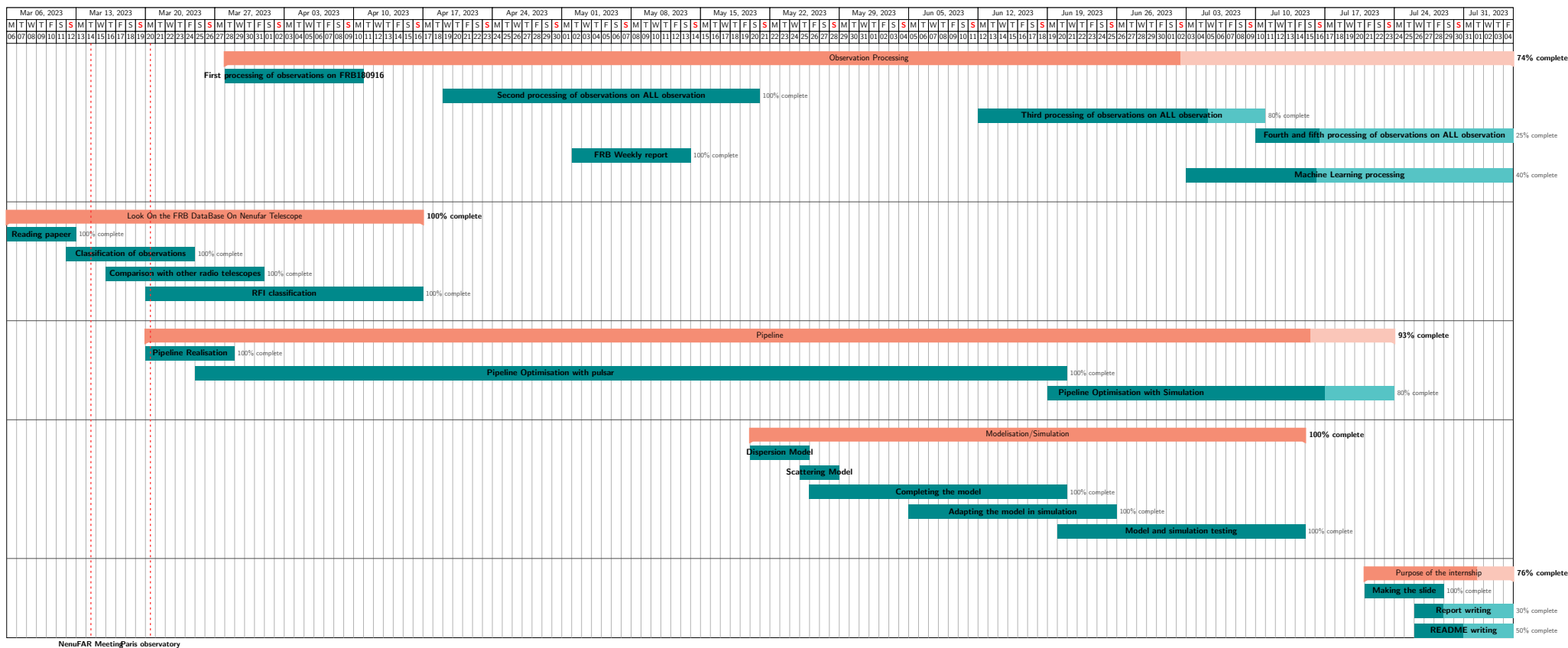
5.1   Gantt internship diagram

Figure 5.1: Annexe 1 : Gantt internship Diagram

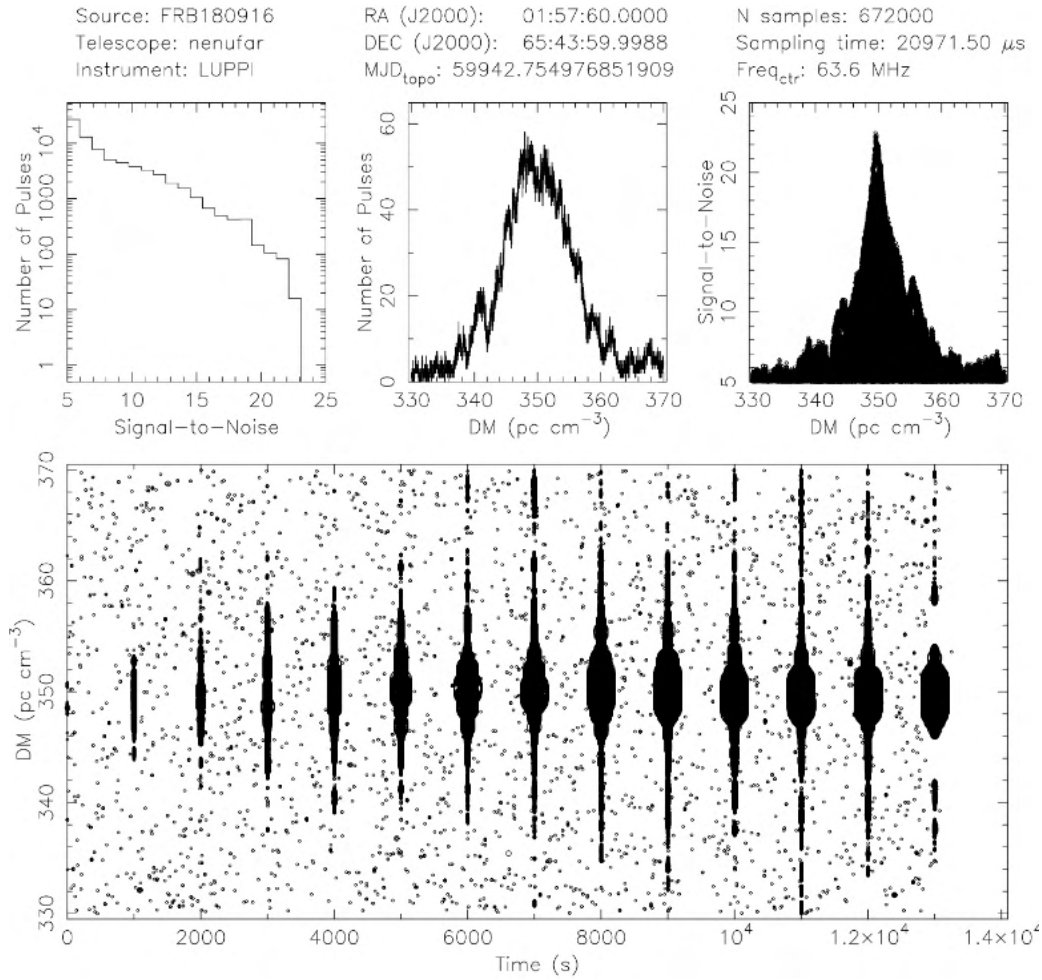## 5.2   Simulated burst amplitude on DM vs Time plot

Figure 5.2: Simulated burst amplitude on DM vs Time plot. This is a plot obtained by superimposing 14 simulations, each introduced every 1000 seconds into the observation, and their amplitudes increasing as the burst moves further into the observation. For this plot, we have taken a block of 1.3 s. It can be seen that pulses close to zero, with energies around 1, are difficult to detect, while larger pulses around 10 are easy to detect. To increase the accuracy of the easy to detect pulses, increasing the size of the blocks makes them easier to detect. This type of plot is used to train the spegid deep learning algorithm, which uses point clouds to generate potential candidates. For example, on this plot, spegid finds all the simulated FRBs except the one introduced at t = 0.
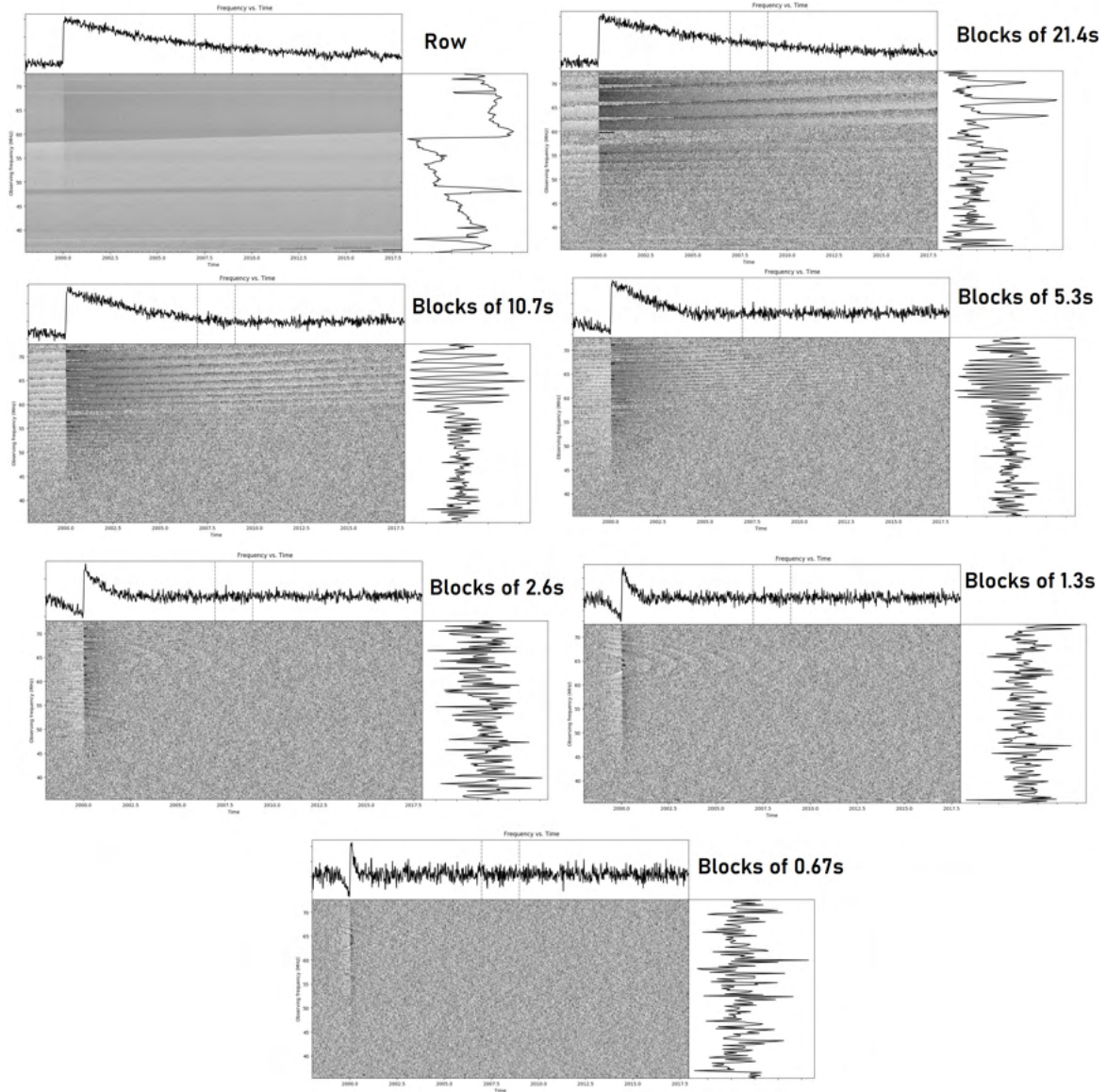
5.3 Block Size Impact

Figure 5.3: Annexe 3 : Block Size Impact. Each plot represents a simulated burst of FRB20220912A presented in section (3.3). It is a dynamic spectrum dedispersed at 218.9 pc.cm^{-3} and each plot is obtained for a processing performed with different block sizes. The same pulse is sent and can be seen in the upper left plot obtained without processing. Note that the dynamic spectrum of this plot is not normalised and has large frequency variations. All the other plots are obtained after the first script of the pipeline with different block sizes. As the study shows, a large block size keeps the pulse clean (top right blocks) but still does not decompose the signal correctly. A very small block size, on the other hand, reduces the burst size considerably. Fewer points per block will inevitably lead to a more brutal normalisation of the signal, as fewer points are considered for the statistics. So we need to find a balance between retaining a strong burst (high SNR) and avoiding retaining too much noise (which lowers the SNR and can lead to non-detection). The block size has to be adapted to the observation and the burst we are trying to detect.
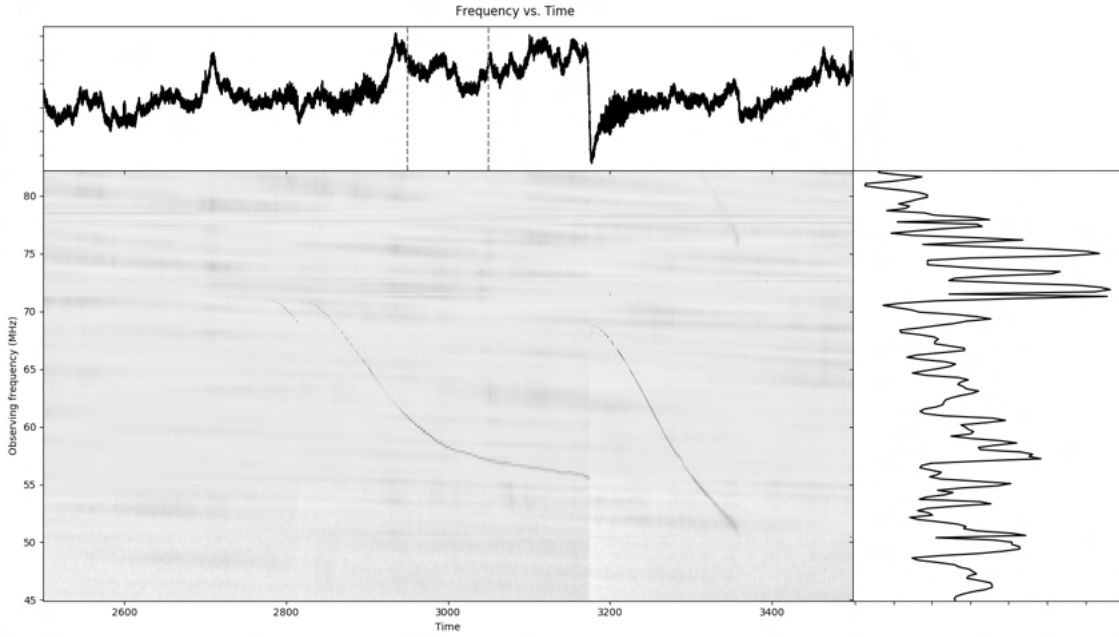
5.4 Interference candidate

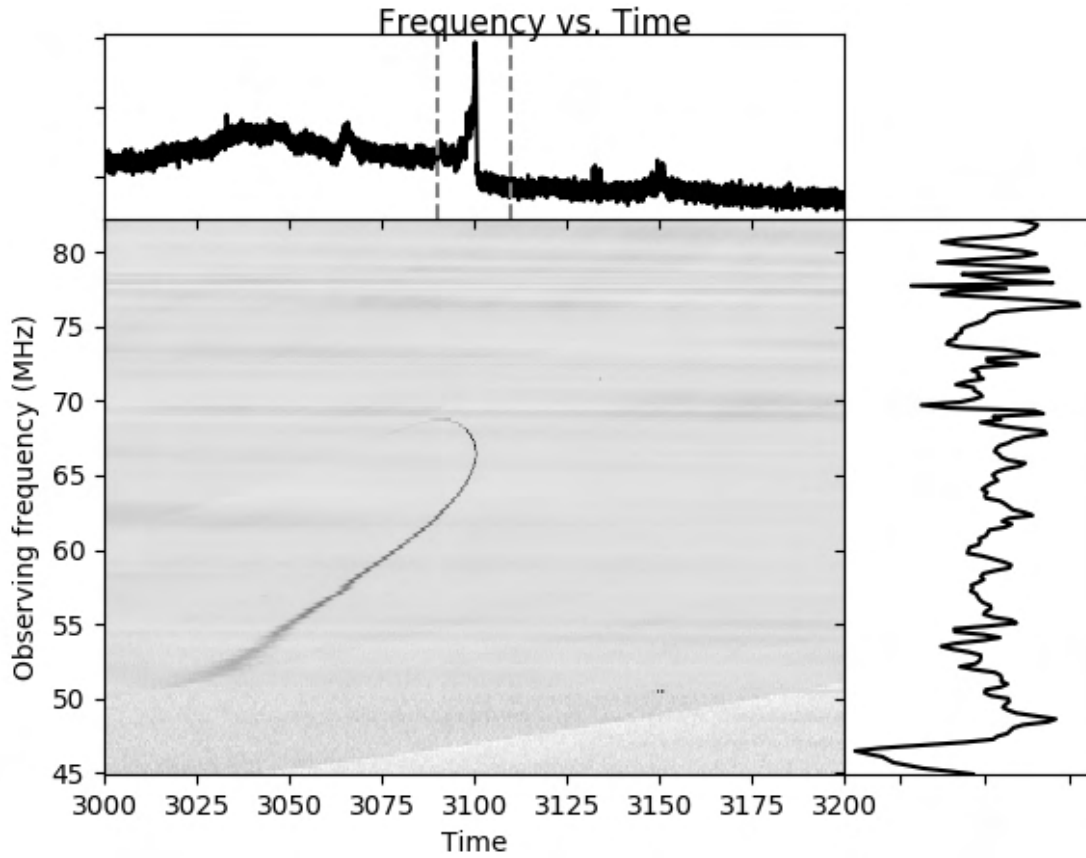Figure 5.4: Dynqmic spectrum of undedispersed interference

Figure 5.5: Dynqmic spectrum of dedispersed interference at 350 pm.cm^{-3}

this interference represents in Fig. 5.4 and Fig. 5.5 what most closely resembles a detection of what we have observed. After discussions with the engineers at the radio telescope site, it

seems that a malfunctioning amplifier is responsible for the shape of the artefact observed. At the moment we're just looking at bright FRB detection. This interference is bright and it's for that reason we detected this one clearly. On the other, the new treatments are dedicated to weak burst. So there are a lot more possible false matchs and we're going to have to find a way of sorting them out efficiently at the request of the machine learning script.

Bibliography

[1] Adam, fetch, https://github.com/CHIME-Pulsar-Timing/fetch

[2] Antoniadis J., et al.,, The second data release from the European Pulsar Timing Array I. The dataset and timing analysis, doi:10.48550/arXiv.2306.16224, https://ui.adsabs.harvard.edu/abs/2023arXiv230616224A

[3] Antoniadis J., et al.,, The second data release from the European Pulsar Timing Array II. Customised pulsar noise models for spatially correlated gravitational waves, doi:10.48550/arXiv.2306.16225, https://ui.adsabs.harvard.edu/abs/2023arXiv230616225A

[4] Astron, LOFAR website, https://www.astron.nl/telescopes/lofar/

[5] Bondonneau L., et al.,,] 10.1051/0004-6361/202039339, 652, A34

[6] Brionne M., Grießmeier J. M., Cognard I., Theureau G., Gros R., Bondonneau L., , The NenuFAR pulsar blind survey. https://ui.adsabs.harvard.edu/abs/2022sf2a.conf..349B

[7] CHIME/FRB Collaboration et al.,,] 10.3847/1538-4365/ac33ab, 257, 59

[8] Chime/Frb Collaboration et al.,,] 10.1038/s41586-020-2398-2, 582, 351

[9] Gaspari P., , Pierre, https://github.com/gasparip

[10] Gopinath A., et al.,, Propagation effects at low frequencies seen in the LOFAR long-term monitoring of the periodically active FRB 20180916B, doi:10.48550/arXiv.2305.06393, https://ui.adsabs.harvard.edu/abs/2023arXiv230506393G

[11] Hessels J. W. T., et al.,,] 10.3847/2041-8213/ab13ae, 876, L23

[12] Kempf S., et al.,, 1683, 1134

[13] Kirsten F., Bhat N. D. R., Meyers B. W., Macquart J. P., Tremblay S. E., Ord S. M., ,] 10.3847/1538-4357/ab0c05, 874, 179

[14] Lorimer D. R., Kramer M., , Handbook of Pulsar Astronomy. Vol. 4, https://ui.adsabs.harvard.edu/abs/2004hpa..book.....L

[15] Luo R., Men Y., Lee K., Wang W., Lorimer D. R., Zhang B., ,] 10.1093/mnras/staa704, 494, 665

[16] Narayan R., ,] 10.1098/rsta.1992.0090, 341, 151

[17] Petroff E., Hessels J. W. T., Lorimer D. R., ,] 10.1007/s00159-019-0116-6, 27, 4

[18] Petroff E., Hessels J. W. T., Lorimer D. R., ,] 10.1007/s00159-022-00139-w, 30, 2

[19] Pleunis Z., et al.,,] 10.3847/2041-8213/abec72, 911, L3

[20] You X. P., et al.,,] 10.1111/j.1365-2966.2007.11617.x, 378, 493

[21] Zhang Y.-K., et al.,, FAST Observations of FRB 20220912A: Burst Properties and Polarization Characteristics, doi:10.48550/arXiv.2304.14665, https://ui.adsabs.harvard.edu/abs/2023arXiv230414665Z

[22] de Nançay O. R., , Nenufar Website, https://nenufar.obs-nancay.fr/

[23] LPC2E website, https://www.lpc2e.cnrs.fr/

[24] ransom s., , Presto, https://github.com/scottransom/presto

Fiche résumé

- Identité de l'étudiant

  Pierre Gaspari

- Filière

  Sicom

- Année universitaire

  2022-2023

- Titre du stage et période

  Searching FRBs with NenuFAR de Mars à Aout 2023

- Logo, nom et adresse postale de l'entreprise/laboratoire

  LPC2E, Orleans, 3 Av. de la Recherche Scientifique, 45071 Orléans

- Prénom, nom du maître de stage et son adresse email

  Jean-Mathias Griessmeier : jean-mathias.griessmeier@cnrs-orleans.fr

  Cherry Ng : cherrywyng@gmail.com

- Prénom et nom du tuteur école

  Ronald Phlypo

Descriptif du stage :

- Recherche de FRBs (Fast Radio Bursts) dans la gamme 10-85 MHz avec le radiotélescope NenuFAR à Nançay

- Analyse de données

- Amélioration des méthodes de traitement des données, en particulier l'élimination d'interférences radio (RFI)

- Algorithmes de recherche automatiques (par exemple type "machine learning")

- Affinement de la stratégie d'observation

- Programmation de nouvelles observations

Moyens mis à disposition

1 Ordinateur Portable plus des appareils éléctroniques (écran,souris,claviers)

2 Carte d'acces au batiment mais aussi au campus

3 Clé d'acces à mon bueau

4 Acces VPN pour accéder au serveur du CNRS à distance.

5 Adresse mail pro

6 Acces au refectoire

Le CNRS m'ayant insérer dans une équipe, il y a avait au quotidien,

1 à 2 étudiant en thèses.

1 à 2 doctorant.

mon maître de stage et mon co-maître de stage.

3 à 4 chercheurs/astronome.